

MOX-Report No. 08/2020

**Polytopic Discontinuous Galerkin methods for the
numerical modelling of flow in porous media with
networks of intersecting fractures**

Antonietti, P. F.; Facciola, C.; Verani, M.

MOX, Dipartimento di Matematica
Politecnico di Milano, Via Bonardi 9 - 20133 Milano (Italy)

mox-dmat@polimi.it

<http://mox.polimi.it>

Polytopic Discontinuous Galerkin methods for the numerical modelling of flow in porous media with networks of intersecting fractures *

Paola F. Antonietti[#], Chiara Facciola[#] and Marco Verani[#]

February 15, 2020

[#] MOX- Laboratory for Modeling and Scientific Computing

Dipartimento di Matematica

Politecnico di Milano

Piazza Leonardo da Vinci 32, 20133 Milano, Italy

`paola.antonietti@polimi.it`, `chiara.facciola@polimi.it`, `marco.verani@polimi.it`

Abstract

We present a numerical approximation of Darcy’s flow through a porous medium that incorporates networks of fractures with non empty intersection. Our scheme employs PolyDG methods, i.e. discontinuous Galerkin methods on general polygonal and polyhedral (polytopic, for short) grids, featuring elements with edges/faces that may be in arbitrary number (potentially unlimited) and whose measure may be arbitrarily small. Our approach is then very well suited to tame the geometrical complexity featured by most of applications in the computational geoscience field. From the modelling point of view, we adopt a reduction strategy that treats fractures as manifolds of codimension one and we employ the primal version of Darcy’s law to describe the flow in both the bulk and in the fracture network. In addition, some physically consistent conditions couple the two problems, allowing for jump of pressure at their interface, and they as well prescribe the behaviour of the fluid along the intersections, imposing pressure continuity and flux conservation. Both the bulk and fracture discretizations are obtained employing the Symmetric Interior Penalty DG method extended to the polytopic setting. The key

*Paola F. Antonietti and Chiara Facciola have been supported by SIR Project n. RBSI14VT0S “PolyPDEs: Non-conforming polyhedral finite element methods for the approximation of partial differential equations” funded by MIUR. Marco Verani has been partially supported by the Italian research grant *Prin 2012* 2012HBLYE4 “Metodologie innovative nella modellistica differenziale numerica” and by INdAM-GNCS.

instrument to obtain a polyDG approximation of the problem in the fracture network is the generalization of the concepts of jump and average at the intersection, so that the contribution from all the fractures is taken into account. We prove the well-posedness of the discrete formulation and perform an error analysis obtaining a priori hp -error estimates. All our theoretical results are validated performing preliminary numerical tests with known analytical solution.

Introduction

This work is concerned with the simulation of Darcian flows through porous media that incorporate networks of fractures with non empty intersection. The focus is on the development and analysis of a numerical approximation that employs PolyDG methods, i.e. discontinuous Galerkin methods on general polygonal and polyhedral (polytopic, for short) grids. In the past decades, increased attention has been given to the efficient implementation of numerical methods for fractured reservoir simulations. The analysis and prediction of the flow is indeed fundamental in many environmental and energy engineering applications, which include petroleum extraction, CO₂ storage in depleted oil fields, isolation of radioactive waste and geothermal energy production, for example. In all the aforementioned applications, fractures severely affect the flow, since they can act as barriers for the fluid (when they are filled with low permeable material), or as conduits (when they have higher permeability than the surrounding medium). Moreover, in many cases the geometry of the fault system can be highly intricate, featuring thousands of fractures, which may also intersect with small angles or be nearly coincident [28].

A first step towards a reduction in the complexity of the simulation is usually taken in the conceptual modelling of the flow: since fractures usually present a small width-to-length ratio, as well as a small relative size with respect to the domain, a popular choice consists in treating them as manifolds of codimension one. The development of this kind of reduced models has been addressed for single-phase flows in several works, for example in [2, 1, 32, 29]. Our main reference will be the model described in [32], which considers for simplicity the case of a single fracture non-immersed in the bulk domain. In the model, the flow in the bulk is governed by Darcy's law, whereas a suitable dimensionally reduced version of the law is formulated on the surface modelling the fracture. Moreover, the exchange of fluid between the fracture and the porous medium is described via some physically consistent coupling conditions. We also remark that both low and large permeable fractures can be handled.

Although the use of dimensionally reduced models avoids the requirement of extremely refined grids inside the fracture domains, realistic simulations still call for high mesh resolution

in these areas, so that all the small geometrical features can be captured without resorting to low-quality elements in the classical sense. The mesh generation process within a classical finite elements approach can then represent a bottleneck in the whole simulation, especially in 3D, as only computational grids composed by tetrahedral/hexahedral/prismatic elements are supported. The same issue can be encountered in many application areas, ranging from fluid-structure interaction, to wave propagation problems, to name a few. This has motivated a huge effort in the past years in the design of numerical methods supporting meshes made of general polytopic elements. A huge reduction on the computational cost may be achieved by resorting to hybrid mesh generation techniques, for example: first a (possibly structured) grid is generated independently of geometric features (e.g., fractures), secondly the elements are cut according to the required pattern. It follows that the final mesh contains arbitrarily shaped elements in the surrounding of such features and is regular far from them. In addition to the simplicity of the procedure described, polytopic meshes present, on average, a much lower number of elements, even on relatively simple geometries, without committing a variational crime [9, 10].

Within this framework, many numerical methods have been developed on top of polytopic meshes in the context of flows in fractured porous media. In particular, we mention [8, 28], where a mixed approximation based on Mimetic Finite Differences was applied; the works [13, 14], where virtual elements were employed to deal with flows in Discrete Fracture Networks, and [22], which uses the Hybrid High-Order method. We also remark that an important alternative is given by the use of non-conforming discretizations, in which the bulk grid can be chosen fairly regular independently from the fractures, since these are considered immersed in the geometry. We refer to [24, 31, 26] for the use of the eXtended Finite Element Method and to [17] for the Cut Finite Element Method.

In [6] we presented an approximation of the coupled bulk-fracture problem that employs PolyDG methods. The inherited flexibility of DG methods in handling arbitrarily shaped, non-necessarily matching, grids and elementwise variable polynomial orders represents, in fact, the ideal setting to handle such kind of problems that typically feature a high-level of geometrical complexity. In particular, since they employ local polynomial spaces defined elementwise without any continuity constraint, DG methods feature a high-level of intrinsic parallelism. Furthermore, the lack of continuity between neighbouring elements allows for the employment of extremely broad families of meshes containing elements with edges/faces that may be in arbitrary number (potentially unlimited) and whose measure may be arbitrarily small. The geometric flexibility highlighted so far is not the only motivation to employ such techniques in the context of fractured porous media. A more physically motivated argument is given by the discontinuous nature of the solution at the matrix-fractures interface, which

can be intrinsically captured in the choice of the discrete spaces. In addition, the bulk and fractures coupling can be easily reformulated by means of the jump and average operators, which are a fundamental tool in the development of DG formulations, and thus naturally incorporated into the variational formulation. Finally, the abstract setting proposed in [12], based on the flux-formulation, allows for the introduction of a unified framework where primal or mixed formulations can be chosen independently for both bulk and fractures, depending on the application at hand and on the quantities of interest. We refer to [7] for further details on the unified analysis and to [6] for a focus on the primal-primal framework. In both cases, our analysis was carried on in the simplified setting of a single, non-immersed fracture. The purpose of the present work is to extend our formulation to networks of *intersecting* fractures. For simplicity, we consider, as in [6], the primal-primal setting, so that we can mainly focus on handling the intersections. To this aim, we supplement the mathematical model [32] with some suitable physical conditions at the intersections, prescribing the behaviour of the fluid. Following [28, 16, 14], we impose that:

- pressure between fractures is continuous along the intersections;
- flux is conserved, so that no exchange of fluid between bulk and fracture network takes place along the intersections.

We mention that more general conditions, where the angle between fractures is taken into account and jumps of pressure across the intersection are allowed, may be imposed. Some examples can be found in [33, 27, 15, 23, 30]. We also mention that the analysis of the mixed-mixed setting in the case of a totally immersed network of fractures has been addressed in [28].

From the DG-discretization point of view, the key instrument for dealing with intersections is the generalization of the concepts of jump and average. If we assume that the fracture network may be approximated by the union of N_Γ fractures γ_k , each of which is a one co-dimensional planar manifold, i.e. $\Gamma = \bigcup_{k=1}^{N_\Gamma} \gamma_k$, the intersections correspond to lines when $d = 3$ and to points when $d = 2$. Let us focus for simplicity on the case $d = 3$, see Figure 1 for an example. Here, the intersection line is denoted by \mathcal{I}_Γ and each fracture γ_k , $k = 1, 2, 3, 4$, is characterised by the outward normal vector $\boldsymbol{\tau}_k$ at the intersection, which belongs to the plane containing the fracture. In order to describe the pressure field in all the network, we employ the global variable $p_\Gamma = (p_\Gamma^1, \dots, p_\Gamma^{N_\Gamma})$, defined in a suitable product space of all the local fracture spaces. Our aim is to introduce some operators that are able to capture the behaviour of the function p_Γ across the intersection line, taking into account the contribution from all the fractures, similarly to how classic jump and average operators [12] describe the discontinuity of a piecewise-continuous function across elemental interfaces. The main

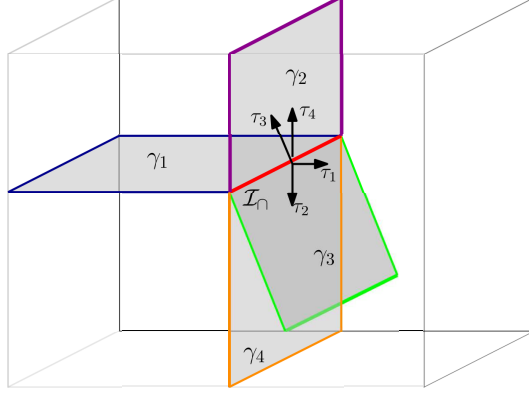


Figure 1: Example of network of intersecting fractures and corresponding normal vectors for $d = 3$.

difference with respect to the standard case is that the normal vectors, contained into the definition of the operators, are not aligned. This is related to the linear DG approximation of elliptic PDEs on surfaces presented in [25], then extended to high order in [5]. Here, the surface is approximated by a piecewise linear surface composed of planar triangles, so that a new definition of jump and average operators is needed, to take into account the fact that the outward normal vectors of two neighbouring triangles are not, in general, opposite. Our definition is a further generalization, since it considers the intersection of an arbitrary number of planar surfaces. Using the newly defined jump and average operators we are able to define a DG approximation for the problem in the bulk combined with a DG approximation for the problem in the fracture network, where the conditions at the intersection are imposed “in the spirit of DG methods”. In particular, this means that continuity is enforced *penalizing the jump* of the pressure (after a suitable definition of the penalization coefficient at the intersection), while balance of fluxes is imposed *naturally*, similarly to how homogeneous Neumann boundary conditions are usually enforced. Both the bulk and fracture discretizations are obtained employing the SIPDG method extended to the polytopic setting.

The rest of the paper is structured as follows. In Section 1, we present the mathematical model. In Section 2, we introduce the weak formulation of the problem and prove its well-posedness. Section 3 contains the polyDG discretization of the coupled system based on the new definition of jump and average operators at intersections, which we introduce in Section 3.1.1. Finally, Sections 4 and 5 enclose the stability and error analysis of the discrete method. We conclude with Section 6, where we present some preliminary numerical experiments with known analytical solution, so that we are able to verify the obtained convergence rates.

1 Mathematical model

We consider the domain $\Omega \subset \mathbb{R}^d$, with $d = 2, 3$, representing the porous medium. We assume that the fracture network may be approximated by a collection of one co-dimensional planar manifolds $\Gamma \subset \mathbb{R}^{d-1}$, adopting the reduced model introduced in [32] and extended to fracture networks in [28, 16, 14]. In particular, we consider Γ to be the union of N_Γ fractures γ_k ,

$$\Gamma = \bigcup_{k=1}^{N_\Gamma} \gamma_k,$$

with every γ_k being an open, bounded, connected, planar $(d-1)$ -dimensional orientable manifold. Each γ_k is, in fact, the approximation of the actual fracture $\tilde{\gamma}_k$, which we assume may be characterized by

$$\tilde{\gamma}_k = \left\{ \mathbf{x} + d\mathbf{n}_k, \text{ for } \mathbf{x} \in \gamma_k, d \in \left(-\frac{\ell_k(\mathbf{x})}{2}, \frac{\ell_k(\mathbf{x})}{2} \right) \right\},$$

where \mathbf{n}_k is a unit normal vector to γ_k , whose precise definition is given below, and $\ell_k(\mathbf{x})$ is a \mathcal{C}^1 function that describes the fracture aperture. For all $k = 1, \dots, N_\Gamma$, we assume there is a constant $\ell_* > 0$ such that $\ell_k > \ell_*$. Finally, we denote by ℓ_Γ the aperture of the whole fracture network, meaning that $\ell_\Gamma|_{\gamma_k} = \ell_k$.

Without loss of generality for the analysis (see Remark 1), we can assume that:

- (i) the fracture network is connected;
- (ii) all the fractures intersect in one point if $d = 2$ or line if $d = 3$;
- (iii) for each fracture, the intersection point corresponds to one of its endpoints if $d = 2$ or to part of one of its facets if $d = 3$.

We denote by \mathcal{I}_\cap the intersection point/line, i.e.,

$$\mathcal{I}_\cap = \bigcap_{k=1}^{N_\Gamma} \tilde{\gamma}_k.$$

We assume that the angle between intersecting fractures is bounded from below, as well as the angles between fractures and $\partial\Omega$, whenever a fracture touches the boundary. This implies, in particular, that the number of fractures joining at the intersection is bounded.

We assume that the boundary of the bulk domain may be subdivided into two measurable subsets for the imposition of boundary conditions on the pressure and on the Darcy's velocity, that is $\partial\Omega = \partial\Omega_D \cup \partial\Omega_N$, with $|\partial\Omega_D| > 0$. This induces a subdivision of the boundary of each fracture into four different sets, some of which may be empty:

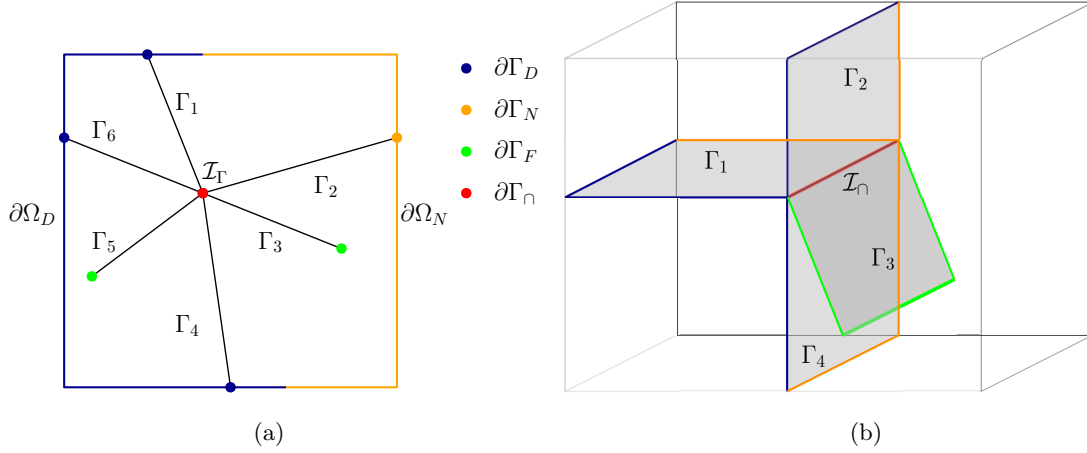


Figure 2: Example of fracture network satisfying the geometrical assumptions with subdivision of the boundary into sets for $d = 2$ (left) and $d = 3$ (right).

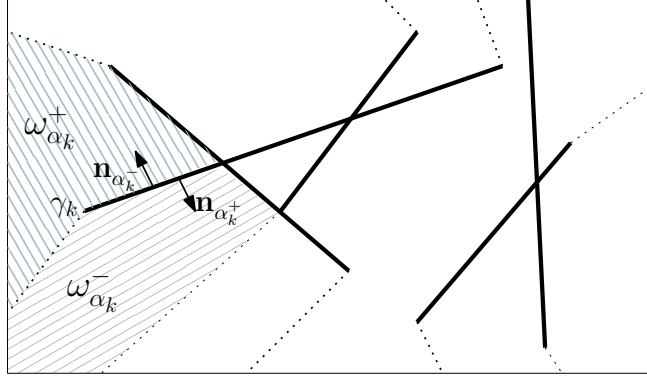


Figure 3: Partition of the domain Ω into subdomains ω_j induced by the prolongation of fractures.

$\partial\gamma_k^D = \partial\gamma_k \cap \partial\Omega_D$, $\partial\gamma_k^N = \partial\gamma_k \cap \partial\Omega_N$, the intersection tips $\partial\gamma_k^\cap = \bigcup_{\substack{j=1 \\ j \neq k}}^{N_\Gamma} (\partial\gamma_k \cap \partial\gamma_j)$ and finally $\partial\gamma_k^F = \partial\gamma_k \setminus (\partial\gamma_k^D \cup \partial\gamma_k^N \cup \partial\gamma_k^\cap)$, which corresponds to the set of immersed tips. We also introduce the corresponding definitions for the network $\partial\Gamma_D = \bigcup_{k=1}^{N_\Gamma} \partial\gamma_k^D$, $\partial\Gamma_N = \bigcup_{k=1}^{N_\Gamma} \partial\gamma_k^N$, $\partial\Gamma_\cap = \bigcup_{k=1}^{N_\Gamma} \partial\gamma_k^\cap$ and $\partial\Gamma_F = \bigcup_{k=1}^{N_\Gamma} \partial\gamma_k^F$. Some of these sets may as well be empty, and also the case of totally immersed network, i.e., $\partial\Gamma_D \cup \partial\Gamma_N = \emptyset$ is admitted. See Figure 2(a)-2(b) for an explicative example of the notation.

Following the same strategy as in [3, 28, 16], we assume that the fractures can be suitably extended so that the domain Ω is partitioned into a collection of Lipschitz subdomains ω_j , with $j = 1, \dots, N_\omega$, i.e., $\Omega = \bigcup_{j=1}^{N_\omega} \omega_j$, cf Figure 3. By construction, for each fracture γ_k we have exactly two subdomains, ω_{α^+} and ω_{α^-} , such that $\gamma_k \subset \partial\omega_{\alpha^+} \cap \partial\omega_{\alpha^-}$. This implies that we can identify for each fracture γ_k the normal \mathbf{n}_k defined as $\mathbf{n}_k = \mathbf{n}_{\alpha^+} = -\mathbf{n}_{\alpha^-}$, where \mathbf{n}_α is the unit normal vector pointing outward of the subdomain ω_α . Moreover, we denote by

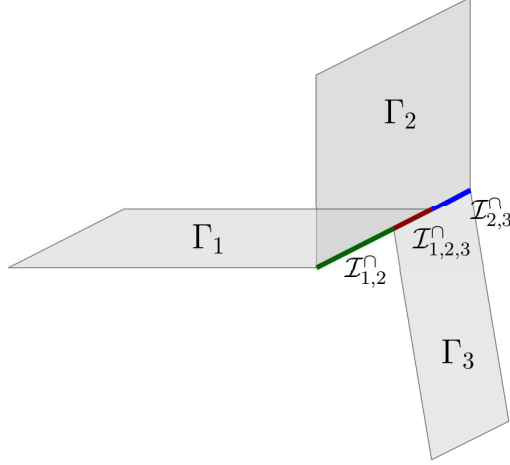


Figure 4: Example of multiple intersections for $d = 3$, where an intersection is defined as a segment shared by a fixed subset of fractures. Here, we can define 3 intersections, $\mathcal{I}_{1,2}^\cap = \partial\Gamma_1 \cap \partial\Gamma_2$, $\mathcal{I}_{1,2,3}^\cap = \partial\Gamma_1 \cap \partial\Gamma_2 \cap \partial\Gamma_3$ and $\mathcal{I}_{2,3}^\cap = \partial\Gamma_2 \cap \partial\Gamma_3$

\mathbf{n}_Γ the normal to the whole fracture network, meaning that $\mathbf{n}_\Gamma = \mathbf{n}_k$ on γ_k .

Then, for a regular-enough scalar-valued function q defined on Ω , we can introduce *jump* and *average* across the fracture $\gamma_k \subset \partial\omega_{\alpha_k^+} \cap \partial\omega_{\alpha_k^-}$ in a standard way as

$$\llbracket q \rrbracket_{\gamma_k} = q_{\alpha_k^+} \mathbf{n}_{\alpha_k^+} + q_{\alpha_k^-} \mathbf{n}_{\alpha_k^-}, \quad \{q\}_{\gamma_k} = \frac{1}{2}(q_{\alpha_k^+} + q_{\alpha_k^-}), \quad (1)$$

where $q_{\alpha_k^+}$ and $q_{\alpha_k^-}$ are the restriction to γ_k of the traces of q on $\partial\omega_{\alpha_k^+}$ and $\partial\omega_{\alpha_k^-}$, respectively. We refer to [16] and to [3] for a rigorous definition of the trace operators, also in the case of immersed tips. Similarly, for a regular-enough vector valued function \mathbf{v} , we define

$$\llbracket \mathbf{v} \rrbracket_{\gamma_k} = \mathbf{v}_{\alpha_k^+} \cdot \mathbf{n}_{\alpha_k^+} + \mathbf{v}_{\alpha_k^-} \cdot \mathbf{n}_{\alpha_k^-}, \quad \{\mathbf{v}\}_{\gamma_k} = \frac{1}{2}(\mathbf{v}_{\alpha_k^+} + \mathbf{v}_{\alpha_k^-}). \quad (2)$$

Moreover, for given functions f_k defined on γ_k , with $k = 1, \dots, N_\Gamma$, we define the function f_Γ on the network Γ , in the sense of product spaces, as $f_\Gamma = \prod_{k=1}^{N_\Gamma} f_k$. We can then define the jump and average of a function q across the fracture network as $\llbracket q \rrbracket_\Gamma = \prod_{k=1}^{N_\Gamma} \llbracket q \rrbracket_{\gamma_k}$ and $\{q\}_\Gamma = \prod_{k=1}^{N_\Gamma} \{q\}_{\gamma_k}$, respectively.

Remark 1. We remark that the geometric hypotheses on the fracture network were made only for the sake of simplicity and the analysis can be easily extended to more general configurations. More precisely, the case of a network featuring multiple connected components can be treated analogously, as long as the partition of Ω into subdomains ω_α is aligned with all of them. The case of multiple intersections is an easy extension when $d = 2$, and the same holds true when $d = 3$ if we define an intersection as a segment shared by a fixed subset of fractures (see Figure 4 for an explicative example). Note that we do not need to

impose any condition at the point shared by two intersections, since we are assuming that no flux is present along the intersections.

1.1 Governing equations

In what follows, we present the governing equations for our model. In accordance with our previous works, [6, 7], we take as a reference the model for single-phase flow derived in [32], where fractures are treated as $(d - 1)$ -dimensional interfaces between d -dimensional subdomains. In particular, we adopt the extension of the above model to fracture networks developed in [28, 16].

The flow of an incompressible fluid through a fractured d -dimensional porous medium, $d = 2, 3$, may be described by four elements:

1. *Governing equations for the flow in the porous medium:*

We assume that the flow is governed by Darcy's law. We denote by p the fluid pressure and by $\boldsymbol{\nu}$ the permeability tensor, which we assume to include also the dependency on the viscosity. Given a function $f \in L^2(\Omega)$ representing a source term and a function $g \in H^{-1/2}(\partial\Omega_D)$, the motion of the fluid in the bulk may be then described by the following equations

$$\begin{aligned} -\nabla \cdot (\boldsymbol{\nu} \nabla p) &= f && \text{in } \Omega \setminus \bar{\Gamma}, \\ p &= g_D && \text{on } \partial\Omega_D, \\ \boldsymbol{\nu} \nabla p \cdot \mathbf{n} &= 0 && \text{on } \partial\Omega_N, \end{aligned} \quad (3)$$

where \mathbf{n} is the unit normal vector pointing outward of Ω . We also make some regularity assumptions on the tensor $\boldsymbol{\nu} = \boldsymbol{\nu}(\mathbf{x}) \in \mathbb{R}^{d \times d}$, requiring that it is symmetric, positive definite, uniformly bounded from below and above and with entries that are bounded, piecewise continuous real-valued functions.

2. *Governing equations for the flow in the fracture network:*

Darcy's law is used also for modelling the flow along the fractures. In order to obtain a reduced model, where fractures are $(d - 1)$ -dimensional objects immersed in a d -dimensional domain, a process of integration of the equations across the fracture aperture ℓ_Γ is carried on, see [32]. Reduced variables for the average pressure $p_\Gamma = (p_\Gamma^1, \dots, p_\Gamma^{N_\Gamma})$ are then defined on each fracture. The flow is also characterized by the permeability tensor $\boldsymbol{\nu}_\Gamma = (\boldsymbol{\nu}_\Gamma^1, \dots, \boldsymbol{\nu}_\Gamma^{N_\Gamma})$, scaled by viscosity. It is assumed that, on each fracture, $\boldsymbol{\nu}_\Gamma^k$ has a block-diagonal structure of the form

$$\boldsymbol{\nu}_\Gamma^k = \begin{bmatrix} \boldsymbol{\nu}_{\gamma_k}^n & 0 \\ 0 & \boldsymbol{\nu}_{\gamma_k}^\tau \end{bmatrix}, \quad (4)$$

when written in its normal and tangential components, $k = 1, \dots, N_\Gamma$. Here, $\boldsymbol{\nu}_{\gamma_k}^\tau \in \mathbb{R}^{(d-1) \times (d-1)}$ is a positive definite, uniformly bounded tensor (it reduces to a positive number for $d = 2$) representing the tangential component of the permeability of the fracture γ_k . Given a source term $f_\Gamma = (f_\Gamma^1, \dots, f_\Gamma^{N_\Gamma}) \in \prod_{k=1}^{N_\Gamma} L^2(\gamma_k)$ and $g_\Gamma \in H^{1/2}(\partial\Gamma_D)$, the governing equations for the fracture flow read

$$\begin{aligned} -\nabla_\tau \cdot (\boldsymbol{\nu}_\Gamma^\tau \ell_\Gamma \nabla_\tau p_\Gamma) &= \ell_\Gamma f_\Gamma - \llbracket \boldsymbol{\nu} \nabla p \rrbracket && \text{in } \Gamma, \\ p_\Gamma &= g_\Gamma && \text{on } \partial\Gamma_D, \\ (\boldsymbol{\nu}_\Gamma^\tau \ell_\Gamma \nabla_\tau p_\Gamma) \cdot \boldsymbol{\tau} &= 0 && \text{on } \partial\Gamma_N, \\ (\boldsymbol{\nu}_\Gamma^\tau \ell_\Gamma \nabla_\tau p_\Gamma) \cdot \boldsymbol{\tau} &= 0 && \text{on } \partial\Gamma_F, \end{aligned} \quad (5)$$

Here, $\boldsymbol{\tau} = (\boldsymbol{\tau}_1, \dots, \boldsymbol{\tau}_{N_\Gamma})$ is defined on each fracture γ_k as the vector in its tangent plane normal to $\partial\gamma_k$, while ∇_τ and $\nabla_\tau \cdot$ denote the tangential gradient and divergence operators, respectively. Note that, when a certain operator is written on quantities defined on the whole network Γ , it should be interpreted as the product of the corresponding operators on each fracture γ_k .

For the condition on the immersed fracture tips, we have taken as a reference [3], where the model developed in [32] has been extended to fully immersed fractures. In particular, we have imposed a homogeneous conditions for the flux, stating that the mass transfer across the immersed tips can be neglected in front of the transversal one.

3. Coupling conditions between bulk and fractures along their interfaces:

Following [32], we provide the interface conditions to account for the exchange of fluid between the fractures and the porous medium:

$$\begin{aligned} -\{\boldsymbol{\nu} \nabla p\} \cdot \mathbf{n}_\Gamma &= \beta_\Gamma \llbracket p \rrbracket \cdot \mathbf{n}_\Gamma && \text{on } \Gamma, \\ -\llbracket \boldsymbol{\nu} \nabla p \rrbracket &= \alpha_\Gamma (\{p\} - p_\Gamma) && \text{on } \Gamma, \end{aligned} \quad (6)$$

where we have introduced

$$\beta_\Gamma = \frac{1}{2\eta_\Gamma}, \quad \alpha_\Gamma = \frac{2}{\eta_\Gamma(2\xi - 1)}, \quad \eta_\Gamma = \frac{\ell_\Gamma}{\nu_\Gamma^n}, \quad (7)$$

with ν_Γ^n being the normal component of the fracture permeability tensor, see (4). Note that these conditions depend on the closure parameter $\xi \neq \frac{1}{2}$, which is related to the assumption made on the pressure profile across the fracture aperture when deriving the reduced model.

4. Conditions at the intersection:

Finally, following [28, 16, 14], at the fracture intersection \mathcal{I}_\cap we enforce pressure continuity and flux conservation:

$$p_\Gamma^1 = p_\Gamma^2 = \dots = p_\Gamma^{N_\Gamma} \quad \text{in } \mathcal{I}_\cap, \quad (8a)$$

$$\sum_{k=1}^{N_\Gamma} \nu_{\gamma_k}^\tau \ell_k \nabla_\tau p_\Gamma^k \cdot \boldsymbol{\tau}_k = 0 \quad \text{in } \mathcal{I}_\cap. \quad (8b)$$

We remark that other possible, more general, conditions might be imposed at the intersection. Some examples may be found in [33, 27, 15, 23, 30], where the angle between fractures at the intersection is included in the model and jumps of pressure across the intersection are allowed.

2 Weak formulation

In this section we introduce the weak formulation of the model problem (3)-(5)-(6)-(8) and prove its well-posedness.

For the sake of simplicity we will assume that *homogeneous* Dirichlet boundary conditions are imposed for both the bulk and fracture problems, i.e., $g_D = 0$ and $g_\Gamma = 0$. The extension to the general non-homogeneous case is straightforward.

First, we introduce the functional setting. We will employ the following notation. For an open, bounded domain $D \subset \mathbb{R}^d$, $d = 2, 3$, we will denote by $H^s(D)$ the standard Sobolev space of order s , for a real number $s \geq 0$. When $s = 0$, we will write $L^2(D)$. The usual norm on $H^s(D)$ will be denoted by $\|\cdot\|_{s,D}$ and the usual seminorm by $|\cdot|_{s,D}$. Given a decomposition of the domain into elements \mathcal{T}_h , we will denote by $H^s(\mathcal{T}_h)$ the standard *broken* Sobolev space, equipped with the broken norm $\|\cdot\|_{s,\mathcal{T}_h}$. Furthermore, we will denote by $\mathbb{P}_k(D)$ the space of polynomials of *total* degree less than or equal to $k \geq 1$ on D . We will employ the symbols \lesssim and \gtrsim meaning that the inequalities hold up to multiplicative constants that are independent of the discretization parameters, but might depend on the physical parameters.

Next, we introduce the functional spaces for our weak formulation. For the bulk and fracture pressure we define the spaces

$$\begin{aligned} Q^b &= \{q \in H^1(\Omega \setminus \bar{\Gamma}) : q = 0 \text{ on } \partial\Omega_D\}, \\ Q^\Gamma &= \{q_\Gamma = (q_\Gamma^1, \dots, q_\Gamma^{N_\Gamma}) \in \prod_{k=1}^{N_\Gamma} H^1(\gamma_k) : q_\Gamma^k = 0 \text{ on } \partial\gamma_k^D \forall k = 1, \dots, N_\Gamma \\ &\quad \text{and } q_\Gamma^1 = \dots = q_\Gamma^{N_\Gamma} \text{ on } \mathcal{I}_\cap\}, \end{aligned}$$

where the trace operators are understood. We remark that the functions in the fracture space Q^Γ have continuous trace at the intersection. We equip the space $Q^b \times Q^\Gamma$ with the norm

$$\|(q, q_\Gamma)\|^2 = \|\nu^{1/2} \nabla q\|_{0,\Omega}^2 + \|(\nu_\Gamma^\tau \ell_\Gamma)^{1/2} \nabla_\tau q_\Gamma\|_{0,\Gamma}^2 + \|\beta_\Gamma^{1/2} \llbracket q \rrbracket\|_{0,\Gamma}^2 + \|\alpha_\Gamma^{1/2} (\{q\} - q_\Gamma)\|_{0,\Gamma}^2,$$

assuming from now on that $\alpha_\Gamma > 0$, that is $\xi > \frac{1}{2}$, see (7). Moreover, we introduce the bilinear form $\mathcal{A} : (Q^b \times Q^\Gamma) \times (Q^b \times Q^\Gamma) \rightarrow \mathbb{R}$ and the linear functional $\mathcal{L} : Q^b \times Q^\Gamma \rightarrow \mathbb{R}$, defined as

$$\begin{aligned} \mathcal{A}((p, p_\Gamma), (q, q_\Gamma)) &= \int_\Omega \nu \nabla p \cdot \nabla q + \int_\Gamma \nu_\Gamma^\tau \ell_\Gamma \nabla_\tau p_\Gamma \cdot \nabla_\tau q_\Gamma \\ &\quad + \int_\Gamma \beta_\Gamma \llbracket p \rrbracket \cdot \llbracket q \rrbracket + \int_\Gamma \alpha_\Gamma (\{p\} - p_\Gamma) (\{q\} - q_\Gamma) \\ \mathcal{L}(q, q_\Gamma) &= \int_\Omega f q + \int_\Gamma \ell_\Gamma f_\Gamma q_\Gamma. \end{aligned}$$

With the above notation, the weak formulation of the model problem (3)-(5)-(6)-(8) reads as follows: Find $(p, p_\Gamma) \in Q^b \times Q^\Gamma$ such that, for all $(q, q_\Gamma) \in Q^b \times Q^\Gamma$

$$\mathcal{A}((p, p_\Gamma), (q, q_\Gamma)) = \mathcal{L}(q, q_\Gamma). \quad (9)$$

We remark that the equivalence, in the distributional sense, of problem (9) to the model problem (3)-(5)-(6)-(8) can be proved using standard distributional arguments. In particular, if we focus on the problem on the fracture network,

We can now prove the following well-posedness result.

Theorem 2.1. *Let $\xi > 1/2$. Then, problem (9) is well-posed.*

Proof. The statement is a direct consequence of Lax-Milgram Theorem and of the regularity of the forcing terms. \square

We remark that the choice of considering a primal-primal setting for both the bulk and fracture problems is made here only for the sake of simplicity. We refer to [28] for the analysis of the mixed-mixed formulation in the case of a *totally immersed* network of fractures.

Next, we focus on the numerical discretization of the problem based on polyDG.

3 PolyDG discretization

In this section we present a numerical discretization for the coupled bulk-network problem that is based on DG methods on polytopic grids. In particular, we discretize

both the bulk and fracture network problems in primal form, employing the Symmetric Interior Penalty DG method [11, 36]. The key idea to obtain a DG discretization will be the generalization of the concepts of jump and average at the intersection point/line, so that we will be able to impose the conditions at the intersection (8) in the spirit of DG methods. In particular, pressure continuity will be enforced penalizing the jump at the intersection, while balance of fluxes will be imposed “naturally”.

We start with the introduction of the notation related to the polytopic discretization of the domains. For the problem in the bulk, consider a family of meshes \mathcal{T}_h made of disjoint open *polygonal/polyhedral* elements which are aligned with the fracture network Γ and also with the decomposition of Ω into subdomains ω_α , $\alpha = 1, \dots, N_\omega$. In particular, any element $E \in \mathcal{T}_h$ cannot be cut by Γ , and, since the subdomains ω_α are disjoint, each element E belongs exactly to one these subdomains.

In order to admit hanging nodes, following [21, 19, 4, 20], we introduce the concept of mesh *interfaces*, which are defined to be the intersection of the $(d - 1)$ -dimensional facets of neighbouring elements. When $d = 3$, interfaces consists in general polygons and we assume that it is possible to subdivide each interface into a set of co-planar triangles. We denote the set of all these triangles, which we call *faces*. When $d = 2$, the interfaces of an element simply consists of line segments, so that the concepts of faces and interfaces coincide. We still denote by \mathcal{F}_h the set of all faces. Following [21, 19, 4, 20], no limitation is imposed on either the number of faces of each polygon $E \in \mathcal{T}_h$ or on the relative size of element faces compared to its diameter.

Each mesh \mathcal{T}_h induces a subdivision of each fracture in the network γ_k into faces, which we will denote by $\gamma_{k,h}$, for $k = 1, \dots, N_\Gamma$. The collection of all the fracture faces is denoted by Γ_h , i.e., $\Gamma_h = \cup_{k=1}^{N_\Gamma} \gamma_{k,h}$. This implies that the set of all the faces \mathcal{F}_h may be decomposed into three subsets, namely,

$$\mathcal{F}_h = \mathcal{F}_h^I \cup \mathcal{F}_h^B \cup \Gamma_h,$$

where \mathcal{F}_h^B is the set of boundary faces, Γ_h is the set of fracture faces defined above, and \mathcal{F}_h^I is the set of interior faces not belonging to the fracture. In addition, we have $\mathcal{F}_h^B = \mathcal{F}_h^D \cup \mathcal{F}_h^N$, where \mathcal{F}_h^D and \mathcal{F}_h^N are the boundary faces contained in $\partial\Omega_D$ and $\partial\Omega_N$, respectively (we assume the decomposition to be matching with the partition of $\partial\Omega$ into $\partial\Omega_D$ and $\partial\Omega_N$).

The induced discretization of the fractures Γ_h contains the faces of the elements of \mathcal{T}_h that share part of their boundary with one or more fractures, so that Γ_h is made up of line segments when $d = 2$ and of triangles when $d = 3$. We observe that, when $d = 3$, the triangles are not necessarily shape-regular and they may present hanging nodes, due

to the fact that the sub-triangulations of each elemental interface is chosen independently from the others. For this reason, we need to extend the concept of *interface* also to the $(d - 2)$ -dimensional facets of elements in Γ_h , defined again as intersection of boundaries of two neighbouring elements. When $d = 2$, the interfaces reduce to points, while when $d = 3$ they consists of line segments. We denote by $\mathcal{E}_{\Gamma,h}$ the set of all the interfaces (edges) of the elements in Γ_h , and we write, accordingly to the previous notation,

$$\mathcal{E}_{\Gamma,h} = \mathcal{E}_{\Gamma,h}^I \cup \mathcal{E}_{\Gamma,h}^B \cup \mathcal{E}_{\Gamma,h}^F \cup \mathcal{E}_{\Gamma,h}^\cap,$$

where:

- $\mathcal{E}_{\Gamma,h}^I$ is the set of interior edges;
- $\mathcal{E}_{\Gamma,h}^B = \mathcal{E}_{\Gamma,h}^D \cup \mathcal{E}_{\Gamma,h}^N$ is the set of edges belonging to the boundaries of the fracture network $\partial\Gamma_D$ and $\partial\Gamma_N$, respectively;
- $\mathcal{E}_{\Gamma,h}^F$ is the set of edges belonging to the immersed tips of the network;
- $\mathcal{E}_{\Gamma,h}^\cap$ is the set of edges on the intersection of the fractures. Note that, since we are considering a network with one single intersection, when $d = 2$ this set consists only of one single point.

We will also write $\mathcal{E}_{\gamma_k,h}^*$, with $*$ $\in \{I, B, F, \cap\}$, to denote the restriction of each of these sets to the fracture γ_k .

For each element $E \in \mathcal{T}_h$, we denote by $|E|$ its measure, by h_E its diameter and we set $h = \max_{E \in \mathcal{T}_h} h_E$. Moreover, given an element $E \in \mathcal{T}_h$, for any face/edge $F \subset \partial E$ we define \mathbf{n}_F as the unit normal vector on F that points outward of E .

Next, we recall that, for scalar and vector-valued functions q and \mathbf{v} that are piecewise smooth on \mathcal{T}_h , it holds on every $F \in \mathcal{F}_h \setminus \mathcal{F}_h^B$:

$$\llbracket q\mathbf{v} \rrbracket = \llbracket \mathbf{v} \rrbracket \{q\} + \{\mathbf{v}\} \cdot \llbracket q \rrbracket, \quad (10)$$

where jump and average operators are defined similarly to (1) and (2). If we define on \mathcal{F}_h^B

$$\llbracket q \rrbracket = q\mathbf{n}_F, \quad \{\mathbf{v}\} = \mathbf{v}, \quad (11)$$

identity (10) implies the following well-known formula [11]:

$$\sum_{E \in \mathcal{T}_h} \int_{\partial E} q\mathbf{v} \cdot \mathbf{n}_E = \int_{\mathcal{F}_h} \{\mathbf{v}\} \cdot \llbracket q \rrbracket + \int_{\mathcal{F}_h \setminus \mathcal{F}_h^B} \llbracket \mathbf{v} \rrbracket \{q\}, \quad (12)$$

where we have used the compact notation $\int_{\mathcal{F}_h} = \sum_{F \in \mathcal{F}_h} \int_F$.

Analogous definitions may be also stated for the fractures. In particular, given an element $F \in \Gamma_h$, with measure $|F|$ and diameter h_F , for any edge $e \subset \partial F$, with $e \in \mathcal{E}_{\Gamma,h}$, we define \mathbf{n}_e as the unit normal vector on e pointing outward of F (it reduces to ± 1 when $d = 2$). Finally, standard jump and average operators across edges $e \in \mathcal{E}_{\Gamma,h}^I \cup \mathcal{E}_{\Gamma,h}^B$ can be defined for (regular enough) scalar and vector-valued functions and an analogous version of formula (12) can be stated, which we will generalize to intersection edges in Proposition 3.2 below.

3.1 Discrete formulation

For simplicity in the forthcoming analysis, we will suppose that the permeability tensors $\boldsymbol{\nu}$ and $\boldsymbol{\nu}_\Gamma$ are piecewise *constant* on mesh elements, i.e., $\boldsymbol{\nu}|_E \in [\mathbb{P}_0(E)]^{d \times d}$ for all $E \in \mathcal{T}_h$, and $\boldsymbol{\nu}_\Gamma|_F \in [\mathbb{P}_0(F)]^{(d-1) \times (d-1)}$ for all $F \in \Gamma_h$.

First, we introduce the finite-dimensional spaces where we will set our discrete problem. For the problem in the bulk we define the broken polynomial space

$$Q_h^b = \{q \in L^2(\Omega) : q|_E \in \mathbb{P}_{k_E}(E) \forall E \in \mathcal{T}_h\}, \quad k_E \geq 1, \forall E \in \mathcal{T}_h.$$

Similarly, on each fracture γ_k , for $k = 1, \dots, N_\Gamma$, we define the space

$$Q_h^{\gamma_k} = \{q_\Gamma^k \in L^2(\gamma_k) : q_\Gamma^k|_F \in \mathbb{P}_{k_F}(F) \forall F \in \gamma_{h,k}\} \quad k_F \geq 1, \forall F \in \gamma_{h,k},$$

so that on the fracture network we can introduce the product space

$$Q_h^\Gamma = \prod_{k=1}^{N_\Gamma} Q_h^{\gamma_k}.$$

For future use in the analysis, we also introduce the DG vector-valued spaces

$$\begin{aligned} \mathbf{W}_h^b &= \{\mathbf{v} \in [L^2(\Omega)]^d : \mathbf{v}|_E \in [\mathbb{P}_{k_E}(E)]^d \forall E \in \mathcal{T}_h\}, & k_E \geq 1, \forall E \in \mathcal{T}_h, \\ \mathbf{W}_h^{\gamma_k} &= \{\mathbf{v}_\Gamma^k \in [L^2(\Gamma)]^{d-1} : \mathbf{v}_\Gamma^k|_F \in [\mathbb{P}_{k_F}(F)]^{d-1} \forall F \in \gamma_{h,k}\}, & k_F \geq 1, \forall F \in \gamma_{h,k}, \\ \mathbf{W}_h^\Gamma &= \prod_{k=1}^{N_\Gamma} \mathbf{W}_h^{\gamma_k}. \end{aligned}$$

In order to derive a DG discrete formulation of problem (9), we make the following regularity assumption.

Assumption 3.1. *We assume that the exact solution (p, p_Γ) of problem (9) is such that:*

- A1. $p \in Q^b \cap H^2(\mathcal{T}_h)$ and $p_\Gamma \in Q^\Gamma \cap H^2(\Gamma_h)$;
- A2. *the normal components of the exact fluxes $\boldsymbol{\nu} \nabla p$ and $\ell_\Gamma \boldsymbol{\nu}_\Gamma^\top \nabla p_\Gamma$ are continuous across mesh interfaces, that is $[[\boldsymbol{\nu} \nabla p]] = 0$ on \mathcal{F}_h^I and $[[\ell_\Gamma \boldsymbol{\nu}_\Gamma^\top \nabla p_\Gamma]] = 0$ on $\mathcal{E}_{\Gamma,h}^I$.*

Moreover, for the forthcoming analysis, we introduce the following extended continuous spaces

$$Q^b(h) = Q_h^b \oplus (Q^b \cap H^2(\mathcal{T}_h)) \quad (13)$$

$$Q^\Gamma(h) = Q_h^\Gamma \oplus (Q^\Gamma \cap H^2(\Gamma_h)). \quad (14)$$

In order to derive a DG formulation for the problem in the bulk, we proceed as in [6, 7]. We obtain the following: Find $p_h \in Q_h^b$ such that for every test function $q \in Q_h^b$ it holds

$$\begin{aligned} & \int_{\mathcal{T}_h} \boldsymbol{\nu} \nabla p_h \cdot \nabla q - \int_{\mathcal{F}_h^I \cup \mathcal{F}_h^D} \{\boldsymbol{\nu} \nabla p_h\} \cdot \llbracket q \rrbracket - \int_{\mathcal{F}_h^I \cup \mathcal{F}_h^D} \{\boldsymbol{\nu} \nabla q\} \cdot \llbracket p_h \rrbracket + \int_{\mathcal{F}_h^I \cup \mathcal{F}_h^D} \sigma_F \llbracket p_h \rrbracket \cdot \llbracket q \rrbracket \\ & + \int_{\Gamma_h} \beta_\Gamma \llbracket p_h \rrbracket \cdot \llbracket q \rrbracket + \int_{\Gamma_h} \alpha_\Gamma (\{p_h\} - p_\Gamma) \{q\} = \int_{\mathcal{T}_h} f q - \int_{\mathcal{F}_h^D} (\boldsymbol{\nu} \nabla q \cdot \mathbf{n}_F - \sigma_F q) g_D, \end{aligned}$$

where we have introduced the discontinuity penalization parameter σ , which is a non-negative bounded function, i.e., $\sigma \in L^\infty(\mathcal{F}_h^I \cup \mathcal{F}_h^D)$. Its precise definition will be given in Definition 4.2 below.

Next, we derive a DG discrete formulation for the problem on the fracture network. For generality, we will write our formulation referring to the case $d = 3$. However, the expressions are valid also when $d = 2$, provided that, when the domain of integration reduces to a point, the integrals are interpreted as evaluations.

First, we focus on a single fracture γ_k . Given a face $F \in \gamma_{k,h}$, we multiply the first equation in (5) for a test function $q_\Gamma^k \in Q_h^{\gamma_k}$ and integrate over F . Summing over all $F \in \gamma_{h,k}$ and integrating by parts, we obtain

$$\int_{\gamma_{h,k}} \boldsymbol{\nu}_{\gamma_k}^\tau \ell_k \nabla_\tau p_\Gamma^k \cdot \nabla_\tau q_\Gamma^k - \sum_{F \in \gamma_{h,k}} \int_{\partial F} q_\Gamma^k \boldsymbol{\nu}_{\gamma_k}^\tau \ell_k \nabla_\tau p_\Gamma^k \cdot \mathbf{n}_F = \int_{\gamma_{h,k}} \ell_k f_\Gamma q_\Gamma^k - \int_{\gamma_{h,k}} \alpha_\Gamma (\{p\} - p_\Gamma^k) q_\Gamma^k,$$

where we have used the second coupling condition in (6) to rewrite $-\llbracket \boldsymbol{\nu} \nabla p \rrbracket = \alpha_\Gamma (\{p\} - p_\Gamma^k)$ in the source term. If we sum over all the fractures γ_k in the network and use identity (12) on each fracture γ_k , we get

$$\begin{aligned} & \int_{\Gamma_h} \boldsymbol{\nu}_\Gamma^\tau \ell_\Gamma \nabla_\tau p_\Gamma \cdot \nabla_\tau q_\Gamma - \int_{\mathcal{E}_{\Gamma,h}^I} \llbracket \boldsymbol{\nu}_\Gamma^\tau \ell_\Gamma \nabla_\tau p_\Gamma \rrbracket \{q_\Gamma\} - \int_{\mathcal{E}_{\Gamma,h}^I \cup \mathcal{E}_{\Gamma,h}^B} \{\boldsymbol{\nu}_\Gamma^\tau \ell_\Gamma \nabla_\tau p_\Gamma\} \cdot \llbracket q_\Gamma \rrbracket \\ & - \sum_{k=1}^{N_\Gamma} \left[\int_{\mathcal{E}_{\gamma_k,h}^F} q_\Gamma^k \boldsymbol{\nu}_{\gamma_k}^\tau \ell_k \nabla_\tau p_\Gamma^k \cdot \boldsymbol{\tau}_k + \int_{\mathcal{E}_{\gamma_k,h}^\cap} q_\Gamma^k \boldsymbol{\nu}_{\gamma_k}^\tau \ell_k \nabla_\tau p_\Gamma^k \cdot \boldsymbol{\tau}_k \right] = \int_{\Gamma_h} \ell_\Gamma f_\Gamma q_\Gamma - \int_{\Gamma_h} \alpha_\Gamma (\{p\} - p_\Gamma) q_\Gamma, \end{aligned}$$

where we recall that $\boldsymbol{\tau}_k$ is the vector tangent to the fracture γ_k , pointing outward of $\partial\gamma_k$, and $\llbracket \cdot \rrbracket$ and $\{\cdot\}$ are the standard jump and average operators defined in (1), (2) and (11).

In order to treat the term defined on the intersection

$$\sum_{k=1}^{N_\Gamma} \int_{\mathcal{E}_{\gamma_k, h}^\cap} d_\Gamma^k \nu_{\gamma_k}^\tau \ell_k \nabla_\tau p_\Gamma^k \cdot \boldsymbol{\tau}_k, \quad (15)$$

we will now extend the definition of jump and average operators to the case when a number of planes intersect along one line ($d = 3$) or when a number of segments intersect in one point ($d = 2$).

3.1.1 Jump and average operators at the intersection

Let $\underline{b} = (b_1, b_2, \dots, b_{N_\Gamma})$ and $\underline{\mathbf{a}} = (\mathbf{a}_1, \mathbf{a}_2, \dots, \mathbf{a}_{N_\Gamma})$ be a scalar and vector-valued functions defined on the network Γ (product space), such that for every $k = 1, \dots, N_\Gamma$ the traces of b_k and \mathbf{a}_k are well defined on the intersection \mathcal{I}_\cap . Moreover, for $k = 1, \dots, N_\Gamma$, let $\boldsymbol{\tau}_k$ be the vector tangent to the fracture γ_k , pointing outward of the intersection point/line \mathcal{I}_\cap .

Definition 3.1. We define *jump* and *average* operators for $\underline{\mathbf{a}}$ and \underline{b} at \mathcal{I}_\cap as

$$\begin{aligned} \{\underline{b}\}_\cap &= \frac{1}{N_\Gamma} (b_1 + b_2 + \dots + b_{N_\Gamma}) \\ \llbracket \underline{b} \rrbracket_\cap &= (b_i - b_k)_{i, k \in \{1, 2, \dots, N_\Gamma\}, i < k} \\ \{\underline{\mathbf{a}}\}_\cap &= \frac{1}{N_\Gamma} (\mathbf{a}_i \cdot \boldsymbol{\tau}_i - \mathbf{a}_k \cdot \boldsymbol{\tau}_k)_{i, k \in \{1, 2, \dots, N_\Gamma\}, i < k} \\ \llbracket \underline{\mathbf{a}} \rrbracket_\cap &= \mathbf{a}_1 \cdot \boldsymbol{\tau}_1 + \mathbf{a}_2 \cdot \boldsymbol{\tau}_2 + \dots + \mathbf{a}_{N_\Gamma} \cdot \boldsymbol{\tau}_{N_\Gamma}, \end{aligned}$$

where trace operators on \mathcal{I}_\cap are understood.

We remark that $\{\underline{b}\}_\cap$ and $\llbracket \underline{\mathbf{a}} \rrbracket_\cap$ are scalar-valued, while $\llbracket \underline{b} \rrbracket_\cap$ and $\{\underline{\mathbf{a}}\}_\cap$ are vector-valued, taking values in $\mathbb{R}^{\binom{N_\Gamma}{2}}$. In particular, for the definition of $\llbracket \underline{b} \rrbracket_\cap$ and $\{\underline{\mathbf{a}}\}_\cap$ we take all the pairs of indices in $\{1, \dots, N_\Gamma\}$ such that the first index is smaller than the second one. This is just one possible way of indicating all the pairs of fractures. Accordingly, these vectors contain $\binom{N_\Gamma}{2} = \frac{N_\Gamma(N_\Gamma-1)}{2}$ elements. For example, for $N_\Gamma = 4$, we have

$$\llbracket \underline{b} \rrbracket_\cap = (b_1 - b_2, b_1 - b_3, b_1 - b_4, b_2 - b_3, b_2 - b_4, b_3 - b_4) \in \mathbb{R}^6,$$

while, for $N_\Gamma = 5$, we have

$$\llbracket \underline{b} \rrbracket_\cap = (b_1 - b_2, b_1 - b_3, b_1 - b_4, b_1 - b_5, b_2 - b_3, b_2 - b_4, b_2 - b_5, b_3 - b_4, b_3 - b_5, b_4 - b_5) \in \mathbb{R}^{10}.$$

The vector-valued case is analogous. Note also that, when $N_\Gamma = 2$, these definitions coincide with the definitions of jump and average operators introduced in [25, 5], for the generalization

of DG methods to curved surfaces. Indeed we have

$$\begin{aligned} \{\underline{b}\}_\cap &= \frac{1}{2}(b_1 + b_2), & \llbracket \underline{b} \rrbracket_\cap &= b_1 - b_2, \\ \{\underline{a}\}_\cap &= \frac{1}{2}(\mathbf{a}_1 \cdot \boldsymbol{\tau}_1 - \mathbf{a}_2 \cdot \boldsymbol{\tau}_2), & \llbracket \underline{a} \rrbracket_\cap &= \mathbf{a}_1 \cdot \boldsymbol{\tau}_1 + \mathbf{a}_2 \cdot \boldsymbol{\tau}_2. \end{aligned}$$

Definition 3.1 allows us to find an equivalent version of identity (10) on the intersection:

Proposition 3.2. *The following identity holds*

$$\llbracket \underline{b\mathbf{a}} \rrbracket_\cap = \llbracket \underline{a} \rrbracket_\cap \{\underline{b}\}_\cap + \{\underline{a}\}_\cap \llbracket \underline{b} \rrbracket_\cap, \quad (16)$$

where the vector-valued function $\underline{b\mathbf{a}}$ is defined as $\underline{b\mathbf{a}} = (b_1 \mathbf{a}_1, b_2 \mathbf{a}_2, \dots, b_{N_\Gamma} \mathbf{a}_{N_\Gamma})$ and \cdot is the standard scalar-product in $\mathbb{R}^{\binom{N_\Gamma}{2}}$.

Proof. By definition we have

$$\llbracket \underline{b\mathbf{a}} \rrbracket_\cap = \sum_{k=1}^{N_\Gamma} b_k \mathbf{a}_k \cdot \boldsymbol{\tau}_k.$$

Moreover, we can write

$$\llbracket \underline{a} \rrbracket_\cap \{\underline{b}\}_\cap = \frac{1}{N_\Gamma} \left(\sum_{k=1}^{N_\Gamma} b_k \right) \left(\sum_{j=1}^{N_\Gamma} \mathbf{a}_j \cdot \boldsymbol{\tau}_j \right) = \frac{1}{N_\Gamma} \sum_{k=1}^{N_\Gamma} (b_k \mathbf{a}_k \cdot \boldsymbol{\tau}_k) + \frac{1}{N_\Gamma} \sum_{k=1}^{N_\Gamma} (b_k \sum_{\substack{j=1 \\ j \neq k}}^{N_\Gamma} \mathbf{a}_j \cdot \boldsymbol{\tau}_j),$$

while we have

$$\begin{aligned} \{\underline{a}\}_\cap \llbracket \underline{b} \rrbracket_\cap &= \frac{1}{N_\Gamma} \sum_{k=1}^{N_\Gamma} \sum_{j=k+1}^{N_\Gamma} (b_k - b_j) (\mathbf{a}_k \cdot \boldsymbol{\tau}_k - \mathbf{a}_j \cdot \boldsymbol{\tau}_j) \\ &= \frac{1}{N_\Gamma} \sum_{k=1}^{N_\Gamma} \sum_{\substack{j=1 \\ j \neq k}}^{N_\Gamma} (b_k - b_j) \mathbf{a}_k \cdot \boldsymbol{\tau}_k \\ &= \frac{1}{N_\Gamma} \sum_{k=1}^{N_\Gamma} \sum_{\substack{j=1 \\ j \neq k}}^{N_\Gamma} b_k \mathbf{a}_k \cdot \boldsymbol{\tau}_k - \frac{1}{N_\Gamma} \sum_{k=1}^{N_\Gamma} \left(\mathbf{a}_k \cdot \boldsymbol{\tau}_k \sum_{\substack{j=1 \\ j \neq k}}^{N_\Gamma} b_j \right) \\ &= \frac{1}{N_\Gamma} \sum_{k=1}^{N_\Gamma} (N_\Gamma - 1) b_k \mathbf{a}_k \cdot \boldsymbol{\tau}_k - \frac{1}{N_\Gamma} \sum_{k=1}^{N_\Gamma} b_k \left(\sum_{\substack{j=1 \\ j \neq k}}^{N_\Gamma} \mathbf{a}_j \cdot \boldsymbol{\tau}_j \right). \end{aligned}$$

This implies

$$\llbracket \underline{a} \rrbracket_\cap \{\underline{b}\}_\cap + \{\underline{a}\}_\cap \llbracket \underline{b} \rrbracket_\cap = \frac{1}{N_\Gamma} \sum_{k=1}^{N_\Gamma} b_k \mathbf{a}_k \cdot \boldsymbol{\tau}_k + \frac{1}{N_\Gamma} \sum_{k=1}^{N_\Gamma} (N_\Gamma - 1) b_k \mathbf{a}_k \cdot \boldsymbol{\tau}_k = \frac{1}{N_\Gamma} \sum_{k=1}^{N_\Gamma} N_\Gamma b_k \mathbf{a}_k \cdot \boldsymbol{\tau}_k,$$

and the proof is concluded. \square

Now we take our focus back to the derivation of a DG discrete formulation for the problem in the fracture network. Using the above definition of jump and average at the intersection 3.1 and identity (16), we can rewrite (15) as

$$\begin{aligned} \sum_{k=1}^{N_\Gamma} \int_{\mathcal{E}_{\gamma_k, h}^\cap} q_\Gamma^k \boldsymbol{\nu}_{\gamma_k}^\tau \ell_k \nabla_\tau p_\Gamma^k \cdot \boldsymbol{\tau}_k &= \int_{\mathcal{E}_{\Gamma, h}^\cap} \llbracket q_\Gamma \boldsymbol{\nu}_\Gamma^\tau \ell_\Gamma \nabla_\tau p_\Gamma \rrbracket_\cap \\ &= \int_{\mathcal{E}_{\Gamma, h}^\cap} \llbracket q_\Gamma \rrbracket_\cap \cdot \{ \boldsymbol{\nu}_\Gamma^\tau \ell_\Gamma \nabla_\tau p_\Gamma \}_\cap + \int_{\mathcal{E}_{\Gamma, h}^\cap} \llbracket \boldsymbol{\nu}_\Gamma^\tau \ell_\Gamma \nabla_\tau p_\Gamma \rrbracket_\cap \{ q_\Gamma \}_\cap. \end{aligned}$$

The formulation on the fracture network becomes

$$\begin{aligned} \int_{\Gamma_h} \boldsymbol{\nu}_\Gamma^\tau \ell_\Gamma \nabla_\tau p_\Gamma \cdot \nabla_\tau q_\Gamma - \int_{\mathcal{E}_{\Gamma, h}^I} \llbracket \boldsymbol{\nu}_\Gamma^\tau \ell_\Gamma \nabla_\tau p_\Gamma \rrbracket \{ q_\Gamma \} - \int_{\mathcal{E}_{\Gamma, h}^I \cup \mathcal{E}_{\Gamma, h}^B} \{ \boldsymbol{\nu}_\Gamma^\tau \ell_\Gamma \nabla_\tau p_\Gamma \} \cdot \llbracket q_\Gamma \rrbracket \\ - \int_{\mathcal{E}_{\Gamma, h}^F} q_\Gamma \boldsymbol{\nu}_\Gamma^\tau \ell_\Gamma \nabla_\tau p_\Gamma \cdot \boldsymbol{\tau} - \int_{\mathcal{E}_{\Gamma, h}^\cap} \llbracket q_\Gamma \rrbracket_\cap \cdot \{ \boldsymbol{\nu}_\Gamma^\tau \ell_\Gamma \nabla_\tau p_\Gamma \}_\cap - \int_{\mathcal{E}_{\Gamma, h}^\cap} \llbracket \boldsymbol{\nu}_\Gamma^\tau \ell_\Gamma \nabla_\tau p_\Gamma \rrbracket_\cap \{ q_\Gamma \}_\cap \\ = \int_{\Gamma_h} \ell_\Gamma f_\Gamma q_\Gamma - \int_{\Gamma_h} \alpha_\Gamma (\{ p \} - p_\Gamma) q_\Gamma. \end{aligned} \quad (17)$$

From the fact that $p \in Q^\Gamma$ satisfies problem (9) and from the regularity Assumption 3.1, it holds:

- $\llbracket \boldsymbol{\nu}_\Gamma^\tau \ell_\Gamma \nabla_\tau p_\Gamma \rrbracket = 0$ on $\mathcal{E}_{\Gamma, h}^I$;
- $\llbracket p_\Gamma \rrbracket = 0$ on $\mathcal{E}_{\Gamma, h}^I$;
- $\boldsymbol{\nu}_\Gamma^\tau \ell_\Gamma \nabla_\tau p_\Gamma \cdot \boldsymbol{\tau} = 0$ on $\mathcal{E}_{\Gamma, h}^F \cup \mathcal{E}_{\Gamma, h}^N$;
- $\llbracket p_\Gamma \rrbracket_\cap = 0$ on $\mathcal{E}_{\Gamma, h}^\cap$;
- $\llbracket \boldsymbol{\nu}_\Gamma^\tau \ell_\Gamma \nabla_\tau p_\Gamma \rrbracket_\cap = 0$ on $\mathcal{E}_{\Gamma, h}^\cap$.

It follows that, for any test function $q_\Gamma \in Q_h^\Gamma$, identity (17) is equivalent to

$$\begin{aligned} \int_{\Gamma_h} \boldsymbol{\nu}_\Gamma^\tau \ell_\Gamma \nabla_\tau p_\Gamma \cdot \nabla_\tau q_\Gamma - \int_{\mathcal{E}_{\Gamma, h}^I \cup \mathcal{E}_{\Gamma, h}^D} \{ \boldsymbol{\nu}_\Gamma^\tau \ell_\Gamma \nabla_\tau p_\Gamma \} \cdot \llbracket q_\Gamma \rrbracket - \int_{\mathcal{E}_{\Gamma, h}^I \cup \mathcal{E}_{\Gamma, h}^D} \{ \boldsymbol{\nu}_\Gamma^\tau \ell_\Gamma \nabla_\tau q_\Gamma \} \cdot \llbracket p_\Gamma \rrbracket \\ - \int_{\mathcal{E}_{\Gamma, h}^\cap} \{ \boldsymbol{\nu}_\Gamma^\tau \ell_\Gamma \nabla_\tau p_\Gamma \}_\cap \cdot \llbracket q_\Gamma \rrbracket_\cap - \int_{\mathcal{E}_{\Gamma, h}^\cap} \{ \boldsymbol{\nu}_\Gamma^\tau \ell_\Gamma \nabla_\tau q_\Gamma \}_\cap \cdot \llbracket p_\Gamma \rrbracket_\cap \\ + \int_{\mathcal{E}_{\Gamma, h}^I \cup \mathcal{E}_{\Gamma, h}^D} \sigma_e^\Gamma \llbracket p_\Gamma \rrbracket \cdot \llbracket q_\Gamma \rrbracket + \int_{\mathcal{E}_{\Gamma, h}^\cap} \sigma_e^\cap \llbracket p_\Gamma \rrbracket_\cap \cdot \llbracket q_\Gamma \rrbracket_\cap \\ = \int_{\Gamma_h} \ell_\Gamma f_\Gamma q_\Gamma + \int_{\Gamma_h} \alpha_\Gamma (\{ p \} - p_\Gamma) q_\Gamma - \int_{\mathcal{E}_{\Gamma, h}^D} (\boldsymbol{\nu}_\Gamma^\tau \ell_\Gamma \nabla_\tau q_\Gamma \cdot \boldsymbol{\tau} - \sigma_e^\Gamma q_\Gamma) g_\Gamma, \end{aligned}$$

where $\sigma^\Gamma \in L^\infty(\mathcal{E}_{\Gamma, h}^I \cup \mathcal{E}_{\Gamma, h}^D)$ and $\sigma^\cap \in L^\infty(\mathcal{E}_{\Gamma, h}^\cap)$ are discontinuity penalization parameters, whose precise definition will be given in 4.3 below.

In conclusion, we obtain the following discrete formulation for the coupled bulk-network problem:

Find $(p_h, p_{\Gamma,h}) \in Q_h^b \times Q_h^\Gamma$ such that

$$\mathcal{A}_h((p_h, p_{\Gamma,h}), (q, q_\Gamma)) = \mathcal{L}_h(q, q_\Gamma) \quad \forall (q, q_\Gamma) \in Q_h^b \times Q_h^\Gamma, \quad (18)$$

where the bilinear form $\mathcal{A}_h : (Q_h^b \times Q_h^\Gamma) \times (Q_h^b \times Q_h^\Gamma) \rightarrow \mathbb{R}$ is defined as

$$\mathcal{A}_h((p_h, p_{\Gamma,h}), (q, q_\Gamma)) = \mathcal{A}_b(p_h, q) + \mathcal{A}_\Gamma(p_{\Gamma,h}, q_\Gamma) + \mathcal{C}((p_h, p_{\Gamma,h}), (q, q_\Gamma)),$$

and the linear functional $\mathcal{L}_h : Q_h^b \times Q_h^\Gamma \rightarrow \mathbb{R}$ is defined as

$$\mathcal{L}_h(q, q_\Gamma) = \mathcal{L}_b(q) + \mathcal{L}_\Gamma(q_\Gamma),$$

with

$$\begin{aligned} \mathcal{A}_b(p_h, q) &= \int_{\mathcal{T}_h} \boldsymbol{\nu} \nabla p_h \cdot \nabla q - \int_{\mathcal{F}_h^I \cup \mathcal{F}_h^D} \{\boldsymbol{\nu} \nabla p_h\} \cdot \llbracket q \rrbracket \\ &\quad - \int_{\mathcal{F}_h^I \cup \mathcal{F}_h^D} \{\boldsymbol{\nu} \nabla q\} \cdot \llbracket p_h \rrbracket + \int_{\mathcal{F}_h^I \cup \mathcal{F}_h^D} \sigma_F \llbracket p_h \rrbracket \cdot \llbracket q \rrbracket \end{aligned}$$

$$\begin{aligned} \mathcal{A}_\Gamma(p_{\Gamma,h}, q_\Gamma) &= \int_{\Gamma_h} \boldsymbol{\nu}_\Gamma^\tau \ell_\Gamma \nabla_\tau p_{\Gamma,h} \cdot \nabla_\tau q_\Gamma \\ &\quad - \int_{\mathcal{E}_{\Gamma,h}^I \cup \mathcal{E}_{\Gamma,h}^D} \{\boldsymbol{\nu}_\Gamma^\tau \ell_\Gamma \nabla_\tau p_{\Gamma,h}\} \cdot \llbracket q_\Gamma \rrbracket - \int_{\mathcal{E}_{\Gamma,h}^I \cup \mathcal{E}_{\Gamma,h}^D} \{\boldsymbol{\nu}_\Gamma^\tau \ell_\Gamma \nabla_\tau q_\Gamma\} \cdot \llbracket p_{\Gamma,h} \rrbracket \\ &\quad - \int_{\mathcal{E}_{\Gamma,h}^\cap} \{\boldsymbol{\nu}_\Gamma^\tau \ell_\Gamma \nabla_\tau p_{\Gamma,h}\}_\cap \cdot \llbracket q_\Gamma \rrbracket_\cap - \int_{\mathcal{E}_{\Gamma,h}^\cap} \{\boldsymbol{\nu}_\Gamma^\tau \ell_\Gamma \nabla_\tau q_\Gamma\}_\cap \cdot \llbracket p_{\Gamma,h} \rrbracket_\cap \\ &\quad + \int_{\mathcal{E}_{\Gamma,h}^I \cup \mathcal{E}_{\Gamma,h}^D} \sigma_e^\Gamma \llbracket p_{\Gamma,h} \rrbracket \cdot \llbracket q_\Gamma \rrbracket + \int_{\mathcal{E}_{\Gamma,h}^\cap} \sigma_e^\cap \llbracket p_{\Gamma,h} \rrbracket_\cap \cdot \llbracket q_\Gamma \rrbracket_\cap \end{aligned}$$

$$\mathcal{C}((p_h, p_{\Gamma,h}), (q, q_\Gamma)) = \int_{\Gamma_h} \beta_\Gamma \llbracket p_h \rrbracket \cdot \llbracket q \rrbracket + \int_{\Gamma_h} \alpha_\Gamma (\{p_h\} - p_{\Gamma,h}) (\{q\} - q_\Gamma),$$

and

$$\begin{aligned} \mathcal{L}_b(q) &= \int_{\mathcal{T}_h} f q - \int_{\mathcal{F}_h^D} (\boldsymbol{\nu} \nabla q \cdot \mathbf{n}_F - \sigma_F q) g_D, \\ \mathcal{L}_\Gamma(q_\Gamma) &= \int_{\Gamma_h} \ell_\Gamma f_\Gamma q_\Gamma - \int_{\mathcal{E}_{\Gamma,h}^D} (\boldsymbol{\nu}_\Gamma^\tau \ell_\Gamma \nabla_\tau q_\Gamma \cdot \boldsymbol{\tau} - \sigma_e^\Gamma q_\Gamma) g_\Gamma. \end{aligned}$$

In the following, in order to simplify the notation, we will drop the subscript τ for the tangent operators on the fracture network.

4 Well-posedness of the discrete formulation

In this section, we prove that formulation (18) is well-posed.

We recall that, for simplicity in the analysis, we are assuming the permeability tensors $\boldsymbol{\nu}$ and $\ell_\Gamma \boldsymbol{\nu}_\Gamma^\tau$ to be piecewise constant. We will employ the following notation $\bar{\boldsymbol{\nu}}_E = |\sqrt{\boldsymbol{\nu}}|_E|_2^2$ and $\bar{\boldsymbol{\nu}}_F^\tau = |\sqrt{\ell_\Gamma \boldsymbol{\nu}_\Gamma^\tau}|_F|_2^2$, where $|\cdot|_2$ denotes the l_2 -norm.

In order to work in a polytopic framework, we need to introduce some technical tools as in [21, 19, 4, 18, 20]. The first tool consists in trace inverse estimates, so that the norm of a polynomial on a polytope's face/edge can be bounded by the norm on the element itself. To this aim, we need to make some regularity assumptions on the mesh.

Definition 4.1. A mesh \mathcal{T}_h is said to be *polytopic-regular* if, for any $E \in \mathcal{T}_h$, there exists a set of non-overlapping (not necessarily shape-regular) d -dimensional simplices $\{S_E^i\}_{i=1}^{n_E}$ contained in E , such that $\bar{F} = \partial \bar{E} \cap \bar{S}_E^i$, for any face $F \subseteq \partial E$, and

$$h_E \lesssim \frac{d|S_E^i|}{|F|}, \quad i = 1, \dots, n_E,$$

with the hidden constant independent of the discretization parameters, the number of faces of the element n_E , and the face measure.

We remark that this definition does not give any restriction on the number of faces per element, nor on their measure.

Assumption 4.1. We assume that \mathcal{T}_h and Γ_h are *polytopic-regular meshes*.

The above assumption allows us to state the following inverse-trace estimate for polytopic elements [18, 20]:

Lemma 4.2. *Let E be a polygon/polyhedron belonging to a mesh satisfying Definition 4.1 and let $v \in \mathbb{P}_{k_E}(E)$. Then, we have*

$$\|v\|_{L^2(\partial E)}^2 \lesssim \frac{(k_E + 1)(k_E + d)}{h_E} \|v\|_{L^2(E)}^2, \quad (19)$$

where the hidden constant depends on the dimension d , but it is independent of the discretization parameters, of the number of faces of the element and of the relative size of the face compared to the diameter k_E of E .

The second fundamental tool to deal with polytopic discretizations, is an appropriate definition of the discontinuity penalization parameter. In particular, this will be instrumental for handling elements with arbitrarily small faces. Following [21, 19, 4, 18, 20], we define the bulk and fracture penalty functions as:

Definition 4.2. The discontinuity-penalization parameter $\sigma : \mathcal{F}_h \cup \mathcal{F}_h^D \rightarrow \mathbb{R}^+$ for the bulk problem is defined facewise as

$$\sigma(\mathbf{x}) = \sigma_0 \begin{cases} \max_{E \in \{E^+, E^-\}} \frac{\bar{\nu}_E(k_E+1)(k_E+d)}{h_E} & \text{if } \mathbf{x} \subset F \in \mathcal{F}_h^I, \bar{F} = \partial\bar{E}^+ \cap \partial\bar{E}^-, \\ \frac{\bar{\nu}_E(k_E+1)(k_E+d)}{h_E} & \text{if } \mathbf{x} \subset F \in \mathcal{F}_h^D, \bar{F} = \partial\bar{E} \cap \partial\bar{\Omega}, \end{cases} \quad (20)$$

with $\sigma_0 > 0$ independent of k_E , $|E|$ and $|F|$.

Definition 4.3. The discontinuity-penalization parameter $\sigma_\Gamma : \mathcal{E}_{\Gamma,h}^I \cup \mathcal{E}_{\Gamma,h}^D \cup \mathcal{E}_{\Gamma,h}^\cap \rightarrow \mathbb{R}^+$ for the fracture problem is defined edgewise as

$$\sigma^\Gamma(\mathbf{x}) = \sigma_0^\Gamma \begin{cases} \max_{F \in \{F^+, F^-\}} \frac{\bar{\nu}_F^\tau(k_F+1)(k_F+d-1)}{h_F} & \text{if } \mathbf{x} \subset e \in \mathcal{E}_{\Gamma,h}^I, \bar{e} = \partial\bar{F}^+ \cap \partial\bar{F}^-, \\ \frac{\bar{\nu}_F^\tau(k_F+1)(k_F+d-1)}{h_F}, & \text{if } \mathbf{x} \subset e \in \mathcal{E}_{\Gamma,h}^D, \bar{e} = \partial\bar{F} \cap \partial\bar{\Gamma}, \\ \max_{F \in \{F^1, \dots, F^{N_\Gamma}\}} \frac{\bar{\nu}_F^\tau(k_F+1)(k_F+d-1)}{h_F} & \text{if } \mathbf{x} \subset e \in \mathcal{E}_{\Gamma,h}^\cap, \bar{e} = \partial\bar{F}^1 \cap \dots \cap \partial\bar{F}^{N_\Gamma}, \end{cases} \quad (21)$$

with $\sigma_0^\Gamma > 0$ independent of k_F , $|F|$ and $|e|$.

Note that the definition of the fracture parameter on the intersection edges will play a crucial role in proving the well-posedness of our method. In the following we will write σ^\cap to denote $\sigma^\Gamma|_{\mathcal{E}_{\Gamma,h}^\cap}$.

Next, we endow the discrete space $Q_h^b \times Q_h^\Gamma$ with the *energy* norm

$$\| \! \| (q, q_\Gamma) \! \| \! \|^2 = \|q\|_{b,DG}^2 + \|q_\Gamma\|_{\Gamma,DG}^2 + \|(q, q_\Gamma)\|_{\mathcal{C}}^2,$$

where

$$\begin{aligned} \|q\|_{b,DG}^2 &= \|\boldsymbol{\nu}^{1/2} \nabla q\|_{0,\mathcal{T}_h}^2 + \|\sigma_F^{1/2} \llbracket q \rrbracket\|_{0,\mathcal{F}_h^I \cup \mathcal{F}_h^D}^2, \\ \|q_\Gamma\|_{\Gamma,DG}^2 &= \|(\boldsymbol{\nu}_\Gamma^\tau \ell_\Gamma)^{1/2} \nabla q_\Gamma\|_{0,\Gamma_h}^2 + \|\sigma_e^{1/2} \llbracket q_\Gamma \rrbracket\|_{0,\mathcal{E}_{\Gamma,h}^I \cup \mathcal{E}_{\Gamma,h}^D \cup \mathcal{E}_{\Gamma,h}^\cap}^2, \\ \|(q, q_\Gamma)\|_{\mathcal{C}}^2 &= \|\beta_\Gamma^{1/2} \llbracket q \rrbracket\|_{0,\Gamma_h}^2 + \|\alpha_\Gamma^{1/2} (\{q\} - q_\Gamma)\|_{0,\Gamma_h}^2. \end{aligned}$$

Remark 2. Since we are assuming that there is a single intersection in the fracture network Γ , we have that $\|\cdot\|_{b,DG}$ is a norm on the bulk space Q_h^b . In the case of a general fracture network, this holds true only if every connected component of $\Omega \setminus \bar{\Gamma}$ does have part of its boundary in $\partial\Omega_D$. Otherwise, $\|\cdot\|_{b,DG}$ is only a seminorm. Similarly, we have that $\|\cdot\|_{\Gamma,DG}$

is a norm on the network space Q_h^Γ , provided that the network is non-immersed, that is $\partial\Gamma_D \neq \emptyset$. However, we remark that, thanks to the coupling term $\|\cdot\|_C$, we have that $\|\cdot\|$ is a norm on $Q_h^b \times Q_h^\Gamma$ for every possible configuration of the fracture network, including the totally immersed case. Moreover, $\|\cdot\|$ is well defined also on the extended space $Q^b(h) \times Q^\Gamma(h)$ introduced in (13)-(14).

Following [21, 19, 4, 18, 6], the analysis will be based on the introduction of an appropriate *inconsistent* formulation and, consequently, on Strang's second Lemma, [35]. To this end, we introduce the following *extensions* of the forms $\mathcal{A}_b(\cdot, \cdot)$ and $\mathcal{A}_\Gamma(\cdot, \cdot)$ and $\mathcal{L}_b(\cdot)$ and $\mathcal{L}_\Gamma(\cdot)$ to the space $Q^b(h) \times Q^\Gamma(h)$:

$$\begin{aligned}
\tilde{\mathcal{A}}_b(p, q) &= \int_{\mathcal{T}_h} \boldsymbol{\nu} \nabla p_h \cdot \nabla q - \int_{\mathcal{F}_h^I \cup \mathcal{F}_h^D} \{ \boldsymbol{\nu} \boldsymbol{\Pi}_{\mathbf{W}_h^b}(\nabla p_h) \} \cdot \llbracket q \rrbracket \\
&\quad - \int_{\mathcal{F}_h^I \cup \mathcal{F}_h^D} \{ \boldsymbol{\nu} \boldsymbol{\Pi}_{\mathbf{W}_h^b}(\nabla q) \} \cdot \llbracket p \rrbracket + \int_{\mathcal{F}_h^I \cup \mathcal{F}_h^D} \sigma_F \llbracket p \rrbracket \cdot \llbracket q \rrbracket \\
\tilde{\mathcal{A}}_\Gamma(p_{\Gamma, h}, q_\Gamma) &= \int_{\Gamma_h} \boldsymbol{\nu}_\Gamma^\tau \ell_\Gamma \nabla p_\Gamma \cdot \nabla q_\Gamma - \int_{\mathcal{E}_{\Gamma, h}^I \cup \mathcal{E}_{\Gamma, h}^D \cup \mathcal{E}_{\Gamma, h}^\Gamma} \{ \boldsymbol{\nu}_\Gamma^\tau \ell_\Gamma \boldsymbol{\Pi}_{\mathbf{W}_\Gamma^\Gamma}(\nabla p_\Gamma) \} \cdot \llbracket q_\Gamma \rrbracket \\
&\quad - \int_{\mathcal{E}_{\Gamma, h}^I \cup \mathcal{E}_{\Gamma, h}^D \cup \mathcal{E}_{\Gamma, h}^\Gamma} \{ \boldsymbol{\nu}_\Gamma^\tau \ell_\Gamma \boldsymbol{\Pi}_{\mathbf{W}_\Gamma^\Gamma}(\nabla q_\Gamma) \} \cdot \llbracket p_\Gamma \rrbracket + \int_{\mathcal{E}_{\Gamma, h}^I \cup \mathcal{E}_{\Gamma, h}^D \cup \mathcal{E}_{\Gamma, h}^\Gamma} \sigma_e^\Gamma \llbracket p_\Gamma \rrbracket \cdot \llbracket q_\Gamma \rrbracket \\
\tilde{\mathcal{L}}_b(q) &= \int_{\mathcal{T}_h} f q - \int_{\mathcal{F}_h^D} (\boldsymbol{\nu} \boldsymbol{\Pi}_{\mathbf{W}_h^b}(\nabla q) \cdot \mathbf{n}_F - \sigma_F q) g_D, \\
\tilde{\mathcal{L}}_\Gamma(q_\Gamma) &= \int_{\Gamma_h} \ell_\Gamma f_\Gamma q_\Gamma - \int_{\mathcal{E}_{\Gamma, h}^D} (\boldsymbol{\nu}_\Gamma^\tau \ell_\Gamma \boldsymbol{\Pi}_{\mathbf{W}_\Gamma^\Gamma}(\nabla q_\Gamma) \cdot \boldsymbol{\tau}_e - \sigma_e^\Gamma q_\Gamma) g_\Gamma.
\end{aligned} \tag{22}$$

They were obtained by replacing the trace of the gradient operators ∇ and ∇_τ with the trace of their L^2 -projection onto the DG vector-valued spaces \mathbf{W}_h^b and \mathbf{W}_h^Γ , respectively. It follows that these newly introduced forms are well-defined on $Q^b(h) \times Q^\Gamma(h)$ and that they coincide with the formers on the discrete space $Q_h^b \times Q_h^\Gamma$. This means, in particular, that we can consider for the analysis the following *equivalent* version of the discrete problem (18): Find $(p_h, p_{h, \Gamma}) \in Q_h^b \times Q_h^\Gamma$ such that

$$\tilde{\mathcal{A}}_h((p_h, p_h^\Gamma), (q, q_\Gamma)) = \tilde{\mathcal{L}}_h(q, q_\Gamma) \quad \forall (q, q_\Gamma) \in Q_h^b \times Q_h^\Gamma, \tag{23}$$

where $\tilde{\mathcal{A}}_h$ is obtained from \mathcal{A}_h by replacing the bilinear forms with their extended versions (22). Note that formulation (23) is no longer consistent due to the discrete nature of the L^2 -projection operators.

Next, we prove that problem (23) extended to the space $Q^b(h) \times Q^\Gamma(h)$ is well-posed. This, on the one hand, will ensure the well-posedness of discrete problem (18) and, on the other hand, will be of future use in the error analysis. We remark that the results involving

the bulk problem, contained in [6] in the case of one single non-immersed fracture, can be easily extended to the case of a network of fractures. For this reason, our focus will mainly be on the fracture problem.

Following [6], one can prove that the bulk bilinear form $\tilde{\mathcal{A}}_b$ is continuous and coercive:

Lemma 4.3. *Let $\sigma : \mathcal{F}_h^I \cup \mathcal{F}_h^D \rightarrow \mathbb{R}^+$ be defined as in (20). Then, if Assumption 4.1 holds, the bilinear form $\tilde{\mathcal{A}}_b(\cdot, \cdot)$ is continuous on $Q^b(h) \times Q^b(h)$ and, provided that σ_0 is sufficiently large, it is also coercive on $Q^b(h) \times Q^b(h)$, i.e.,*

$$\tilde{\mathcal{A}}_b(p, q) \lesssim \|q\|_{b,DG} \|p\|_{b,DG}, \quad \tilde{\mathcal{A}}_b(q, q) \gtrsim \|q\|_{b,DG}^2,$$

for any $q, p \in Q^b(h)$.

Proof. We refer to Lemma 7.4 in [6]. □

Next, we prove an analogous result for the problem in fracture network.

Lemma 4.4. *Let $\sigma^\Gamma : \mathcal{E}_{\Gamma,h}^I \cup \mathcal{E}_{\Gamma,h}^D \cup \mathcal{E}_{\Gamma,h}^\cap \rightarrow \mathbb{R}^+$ be defined as in (21). Then, if Assumption 4.1 holds, the bilinear form $\tilde{\mathcal{A}}_\Gamma(\cdot, \cdot)$ is continuous on $Q^\Gamma(h) \times Q^\Gamma(h)$ and, provided that σ_0^Γ is sufficiently large, it is also coercive on $Q^\Gamma(h) \times Q^\Gamma(h)$, i.e.,*

$$\tilde{\mathcal{A}}_\Gamma(p_\Gamma, q_\Gamma) \lesssim \|q_\Gamma\|_{\Gamma,DG} \|p_\Gamma\|_{\Gamma,DG}, \quad \tilde{\mathcal{A}}_\Gamma(q_\Gamma, q_\Gamma) \gtrsim \|q_\Gamma\|_{\Gamma,DG}^2,$$

for any $q_\Gamma, p_\Gamma \in Q^\Gamma(h)$.

Proof. We start with coercivity. For any $q_\Gamma \in Q^\Gamma(h)$, we have

$$\begin{aligned} \tilde{\mathcal{A}}_\Gamma(q_\Gamma, q_\Gamma) &= \|q_\Gamma\|_{DG}^2 - 2 \int_{\mathcal{E}_{\Gamma,h}^I \cup \mathcal{E}_{\Gamma,h}^D} \{\boldsymbol{\nu}_\Gamma^\tau \ell_\Gamma \mathbf{\Pi}_{\mathbf{W}_h^\Gamma}(\nabla q_\Gamma)\} \cdot \llbracket q_\Gamma \rrbracket - 2 \int_{\mathcal{E}_{\Gamma,h}^\cap} \{\boldsymbol{\nu}_\Gamma^\tau \ell_\Gamma \mathbf{\Pi}_{\mathbf{W}_h^\Gamma}(\nabla q_\Gamma)\} \cap \cdot \llbracket q_\Gamma \rrbracket \cap \\ &= I + II + III \end{aligned} \tag{24}$$

In order to bound term II, we proceed as in [6], Lemma 7.4. We employ Cauchy-Schwarz's, triangular and Young's inequalities to write:

$$\int_{\mathcal{E}_{\Gamma,h}^I \cup \mathcal{E}_{\Gamma,h}^D} \{\boldsymbol{\nu}_\Gamma^\tau \ell_\Gamma \mathbf{\Pi}_{\mathbf{W}_h^\Gamma}(\nabla q_\Gamma)\} \cdot \llbracket q_\Gamma \rrbracket \lesssim \sum_{\mathcal{E}_{\Gamma,h}^I \cup \mathcal{E}_{\Gamma,h}^D} \left[\varepsilon \int_e (\sigma_e^\Gamma)^{-1} \{\boldsymbol{\nu}_\Gamma^\tau \ell_\Gamma \mathbf{\Pi}_{\mathbf{W}_h^\Gamma}(\nabla q_\Gamma)\}^2 + \frac{1}{4\varepsilon} \int_e \sigma_e^\Gamma \llbracket q_\Gamma \rrbracket^2 \right].$$

From inverse inequality (4.2), the definition of the penalty parameter σ^Γ (21), Assumption 4.1 and the L^2 -stability of the projector $\mathbf{\Pi}_{\mathbf{W}_h^\Gamma}$, we obtain

$$\int_{\mathcal{E}_{\Gamma,h}^I \cup \mathcal{E}_{\Gamma,h}^D} \{\boldsymbol{\nu}_\Gamma^\tau \ell_\Gamma \mathbf{\Pi}_{\mathbf{W}_h^\Gamma}(\nabla q_\Gamma)\} \cdot \llbracket q_\Gamma \rrbracket \lesssim \frac{\varepsilon}{\sigma_{0,\Gamma}} \|(\boldsymbol{\nu}_\Gamma^\tau \ell_\Gamma)^{1/2} \nabla q_\Gamma\|_{0,\Gamma_h}^2 + \frac{1}{4\varepsilon} \|\sigma_e^{1/2} \llbracket q_\Gamma \rrbracket\|_{0,\mathcal{E}_{\Gamma,h}^I \cup \mathcal{E}_{\Gamma,h}^D}^2. \tag{25}$$

We now consider the intersection term III. Multiplying and dividing by σ^\cap and applying Cauchy-Schwarz's and Young's inequalities we have

$$\int_{\mathcal{E}_{\Gamma,h}^\cap} \{\boldsymbol{\nu}_\Gamma^\tau \ell_\Gamma \mathbf{\Pi}_{\mathbf{W}_h^\Gamma}(\nabla q_\Gamma)\}_\cap \cdot \llbracket q_\Gamma \rrbracket_\cap \lesssim \sum_{e \in \mathcal{E}_{\Gamma,h}^\cap} \left[\varepsilon \int_e (\sigma_e^\cap)^{-1} \{\boldsymbol{\nu}_\Gamma^\tau \ell_\Gamma \mathbf{\Pi}_{\mathbf{W}_h^\Gamma}(\nabla q_\Gamma)\}_\cap^2 + \frac{1}{4\varepsilon} \int_e \sigma_e^\cap \llbracket q_\Gamma \rrbracket_\cap^2 \right]. \quad (26)$$

Using the definition of $\{\cdot\}_\cap$ (3.1) and triangular inequality, we obtain

$$\begin{aligned} \int_e \sigma_\cap^{-1} \{\boldsymbol{\nu}_\Gamma^\tau \ell_\Gamma \mathbf{\Pi}_{\mathbf{W}_h^\Gamma}(\nabla q_\Gamma)\}_\cap^2 &= \frac{1}{N_\Gamma} \sum_{\substack{i,k=1 \\ i < k}}^{N_\Gamma} \int_e (\sigma_e^\cap)^{-1} (\boldsymbol{\nu}_{\gamma_i}^\tau \ell_i \mathbf{\Pi}_{\mathbf{W}_h^{\gamma_i}}(\nabla q_\Gamma^i) \cdot \boldsymbol{\tau}_i - \boldsymbol{\nu}_{\gamma_k}^\tau \ell_k \mathbf{\Pi}_{\mathbf{W}_h^{\gamma_k}}(\nabla q_\Gamma^k) \cdot \boldsymbol{\tau}_k)^2 \\ &\leq \frac{2}{N_\Gamma} \sum_{\substack{i,k=1 \\ i < k}}^{N_\Gamma} \left[\int_e (\sigma_e^\cap)^{-1} (\boldsymbol{\nu}_{\gamma_i}^\tau \ell_i \mathbf{\Pi}_{\mathbf{W}_h^{\gamma_i}}(\nabla q_\Gamma^i) \cdot \boldsymbol{\tau}_i)^2 + \int_e (\sigma_e^\cap)^{-1} (\boldsymbol{\nu}_{\gamma_k}^\tau \ell_k \mathbf{\Pi}_{\mathbf{W}_h^{\gamma_k}}(\nabla q_\Gamma^k) \cdot \boldsymbol{\tau}_k)^2 \right] \\ &= \frac{2(N_\Gamma - 1)}{N_\Gamma} \sum_{k=1}^{N_\Gamma} \int_e (\sigma_e^\cap)^{-1} (\boldsymbol{\nu}_{\gamma_k}^\tau \ell_k \mathbf{\Pi}_{\mathbf{W}_h^{\gamma_k}}(\nabla q_\Gamma^k) \cdot \boldsymbol{\tau}_k)^2, \end{aligned}$$

where the last equality follows from the fact that every term appears in the sum exactly $(N_\Gamma - 1)$ times. Since we are assuming that $\ell_\Gamma \boldsymbol{\nu}_\Gamma^\Gamma$ is constant on each $F \in \Gamma_h$, this implies that

$$\begin{aligned} (a) &:= \sum_{e \in \mathcal{E}_{\Gamma,h}^\cap} \int_e \sigma_\cap^{-1} \{\boldsymbol{\nu}_\Gamma^\tau \ell_\Gamma \mathbf{\Pi}_{\mathbf{W}_h^\Gamma}(\nabla q_\Gamma)\}_\cap^2 \leq \varepsilon \frac{2(N_\Gamma - 1)}{N_\Gamma} \sum_{k=1}^{N_\Gamma} \sum_{\substack{F \in \gamma_{k,h} \\ \partial F \cap \mathcal{I}_\cap \neq \emptyset}} \int_{\partial F} \sigma_\cap^{-1} (\boldsymbol{\nu}_{\gamma_k}^\tau \ell_k \mathbf{\Pi}_{\mathbf{W}_h^{\gamma_k}}(\nabla q_\Gamma^k))^2 \\ &\leq \varepsilon \frac{2(N_\Gamma - 1)}{N_\Gamma} \sum_{k=1}^{N_\Gamma} \sum_{\substack{F \in \gamma_{k,h} \\ \partial F \cap \mathcal{I}_\cap \neq \emptyset}} \frac{1}{\sigma_{0,\Gamma}} \left(\frac{\bar{\boldsymbol{\nu}}_F^\tau (k_F + 1)(k_F + d - 1)}{h_F} \right)^{-1} \bar{\boldsymbol{\nu}}_F^\tau \|(\boldsymbol{\nu}_\Gamma^\tau \ell_\Gamma)^{1/2} \nabla q_\Gamma^k\|_{0,\partial F}^2, \end{aligned}$$

where we have employed the definition of σ^Γ and the fact that for all $e \subseteq \partial F$

$$\sigma_e^\Gamma \geq \sigma_{0,\Gamma} \frac{\bar{\boldsymbol{\nu}}_F^\tau (k_F + 1)(k_F + d - 1)}{h_F}.$$

Note that this is also true if $e \subseteq \mathcal{I}_\cap$. Finally, employing inverse inequality (4.2) and the stability of the projection operator $\mathbf{\Pi}_{\mathbf{W}_h^\Gamma}$ we have

$$(a) \lesssim \frac{\varepsilon}{\sigma_{0,\Gamma}} \|(\boldsymbol{\nu}_\Gamma^\tau \ell_\Gamma)^{1/2} \nabla q_\Gamma\|_{0,\Gamma_h}^2. \quad (27)$$

From (24), employing the derived bounds (25), (26) and (27), we obtain that the bilinear $\tilde{\mathcal{A}}_\Gamma(\cdot, \cdot)$ form is coercive, provided that the parameter $\sigma_{0,\Gamma}$ is chosen big enough. Continuity can be proved with analogous arguments. \square

Employing Lemma 4.3 and Lemma 4.4, we can now prove the well-posedness of the discrete problem (18).

Proposition 4.5. *Let the penalization parameters σ for the problem in the bulk and in the fracture network be defined as in (20) and (21), respectively. Then, problem (18) is well-posed, provided that σ_0 and $\sigma_{0,\Gamma}$ are chosen big enough.*

Proof. In order to use Lax-Milgram Theorem, we prove that the bilinear form $\tilde{\mathcal{A}}_h(\cdot, \cdot)$ is continuous and coercive on $Q^b(h) \times Q^\Gamma(h)$. We have, from Cauchy-Schwarz's inequality

$$\begin{aligned} \mathcal{C}((q, q_\Gamma), (q, q_\Gamma)) &= \|(q, q_\Gamma)\|_{\mathcal{C}}^2 \\ \mathcal{C}((q, q_\Gamma), (p, p_\Gamma)) &\leq \sum_{F \in \Gamma_h} \|\beta_\Gamma^{1/2} \llbracket q \rrbracket\|_{L^2(F)}^2 \|\beta_\Gamma^{1/2} \llbracket p \rrbracket\|_{L^2(F)}^2 \\ &\quad + \sum_{F \in \Gamma_h} \|\alpha_\Gamma^{1/2} (\{q\} - q_\Gamma)\|_{L^2(F)}^2 \|\alpha_\Gamma^{1/2} (\{p\} - p_\Gamma)\|_{L^2(F)}^2 \\ &\leq \|(q, q_\Gamma)\| \cdot \|(p, p_\Gamma)\|, \end{aligned}$$

so that coercivity and continuity are a direct consequence of the definition of the norm $\|\cdot\|$ and of Lemmas 4.3 and 4.4. The continuity of the linear operator $\tilde{\mathcal{L}}_h(\cdot)$ can be easily proved by using the Cauchy-Schwarz inequality, thanks to the regularity assumptions on the forcing terms f and f_Γ and on the boundary data g_D and g_Γ . \square

5 Error analysis

In this section, we derive a-priori error estimates for the discrete problem (18). To this aim, in the following, we summarize the results contained in [21, 19, 4, 18, 20], where standard hp -approximation bounds on simplices are extended to arbitrary polytopic elements. These results are indeed the basic tool for the error analysis of DG-methods.

5.1 hp -approximation bounds

All the theory is based on the existence of a suitable covering of the polytopic mesh, made of a set of overlapping simplices [20]:

Definition 5.1. A *covering* $\mathcal{T}_\# = \{T_E\}$ related to the polytopic mesh \mathcal{T}_h is a set of shape-regular d -dimensional simplices T_E , such that for each $E \in \mathcal{T}_h$, there exists a $T_E \in \mathcal{T}_\#$ such that $E \subsetneq T_E$.

Assumption 5.1. [21, 19, 4, 18, 20] *There exists a covering $\mathcal{T}_\#$ of \mathcal{T}_h and a positive constant O_Ω , independent of the mesh parameters, such that*

$$\max_{E \in \mathcal{T}_h} \text{card}\{E' \in \mathcal{T}_h : E' \cap T_E \neq \emptyset, T_E \in \mathcal{T}_\# \text{ s.t. } E \subset T_E\} \leq O_\Omega,$$

and $h_{T_E} \lesssim h_E$ for each pair $E \in \mathcal{T}_h$ and $T_E \in \mathcal{T}_\#$, with $E \subset T_E$.

Moreover, there exists a covering $\mathcal{F}_\#$ of Γ_h and a positive constant O_Γ , independent of the mesh parameters, such that

$$\max_{F \in \Gamma_h} \text{card}\{F' \in \Gamma_h : F' \cap T_F \neq \emptyset, T_F \in \mathcal{F}_\# \text{ s.t. } F \subset T_F\} \leq O_\Gamma,$$

and $h_{T_F} \lesssim h_F$ for each pair $F \in \Gamma_h$ and $T_F \in \mathcal{F}_\#$, with $F \subset T_F$.

From this assumption and standard results for simplices, we can state the following approximation result:

Lemma 5.2. [21, 19, 4, 18, 20] *Let $E \in \mathcal{T}_h$, $F \subset \partial E$ denote one of its faces, and $T_E \in \mathcal{T}_\#$ denote the corresponding simplex such that $E \subset T_E$ (see Definition 5.1). Suppose that $v \in L^2(\Omega)$ is such that $\mathcal{E}v|_{T_E} \in H^{r_E}(T_E)$, for some $r_E \geq 0$. Then, if Assumption 4.1 and 5.1 are satisfied, there exists $\tilde{\Pi}v$, such that $\tilde{\Pi}v|_E \in \mathbb{P}_{k_E}(E)$, and the following bound holds*

$$\|v - \tilde{\Pi}v\|_{H^q(E)} \lesssim \frac{h_E^{s_E - q}}{k_E^{r_E - q}} \|\mathcal{E}v\|_{H^{r_E}(T_E)}, \quad 0 \leq q \leq r_E. \quad (28)$$

Moreover, if $r_E > 1/2$,

$$\|v - \tilde{\Pi}v\|_{L^2(\partial E)} \lesssim \frac{h_E^{s_E - 1/2}}{k_E^{r_E - 1/2}} \|\mathcal{E}v\|_{H^{r_E}(T_E)}. \quad (29)$$

Here, $s_E = \min(k_E + 1, r_E)$ and the hidden constants depend on the shape-regularity of T_E , but are independent of v , h_E , k_E and the number of faces per element, while \mathcal{E} is the continuous extension operator as defined in [34].

Proof. See [21] for a detailed proof of (28) and [18] for the proof of (29). \square

Clearly, analogous approximation results can be stated for the fracture faces, if Assumptions 4.1 and 5.1 are both satisfied.

5.2 Error estimates

For each subdomain ω_j , $j = 1, \dots, N_\omega$, we denote by \mathcal{E}_j the classical continuous extension operator (cf. [34], see also [6]) $\mathcal{E}_j : H^s(\Omega_j) \rightarrow H^s(\mathbb{R}^d)$, for $s \in \mathbb{N}_0$. Similarly, we denote by \mathcal{E}_{γ_k} the continuous extension operator $\mathcal{E}_{\gamma_k} : H^s(\gamma_k) \rightarrow H^s(\mathbb{R}^{d-1})$, for $s \in \mathbb{N}_0$. We then make the following regularity assumptions for the exact solution (p, p_Γ) of problem (9):

Assumption 5.3. *Let $\mathcal{T}_\# = \{T_E\}$ and $\mathcal{F}_\# = \{T_F\}$ denote the associated coverings of Ω and Γ , respectively, of Definition 5.1. We assume that the exact solution (p, p_Γ) is such that:*

- A1. for every $E \in \mathcal{T}_h$, if $E \subset \omega_j$ and p_j denotes the restriction of p to ω_j , it holds $\mathcal{E}_j p_j|_{T_E} \in H^{r_E}(T_E)$, with $r_E \geq 1 + d/2$ and $T_E \in \mathcal{T}_\#$ with $E \subset T_E$;
- A2. for every $F \in \Gamma_h$, if $F \subset \gamma_k$, it holds $\mathcal{E}_{\gamma_k} p_\Gamma^k|_{T_F} \in H^{r_F}(T_F)$, with $r_F \geq 1 + (d-1)/2$ and $T_F \in \mathcal{F}_\#$ with $F \subset T_F$.

From Proposition 4.5 and Strang's second Lemma directly follows this abstract error bound.

Lemma 5.4. *Assuming that the hypotheses of Proposition 4.5 are satisfied, it holds*

$$|||(p, p_\Gamma) - (p_h, p_{\Gamma,h})||| \lesssim \inf_{(q, q_\Gamma) \in Q_h^b \times Q_\Gamma^b} |||(p, p_\Gamma) - (q, q_\Gamma)||| + \sup_{(w, w_\Gamma) \in Q_h^b \times Q_\Gamma^b} \frac{|\mathcal{R}_h((p, p_\Gamma), (w, w_\Gamma))|}{|||(w, w_\Gamma)|||},$$

where the residual \mathcal{R}_h is defined as

$$\mathcal{R}_h((p, p_\Gamma), (w, w_\Gamma)) = \tilde{\mathcal{A}}_h((p, p_\Gamma), (w, w_\Gamma)) - \tilde{\mathcal{L}}_h(w, w_\Gamma).$$

It is easy to show that the residual is the sum of two contributions, one involving only the bulk problem and one involving only the network problem:

$$\mathcal{R}_h((p, p_\Gamma), (w, w_\Gamma)) = \mathcal{R}_b(p, w) + \mathcal{R}_\Gamma(p_\Gamma, w_\Gamma) \quad (30)$$

It follows that, to derive a bound for the global residual, we can bound each of the two contributions separately. Again, we will focus mainly on the term related to the fracture network.

Lemma 5.5. *Let (p, p_Γ) be the exact solution of problem (9) satisfying the regularity Assumptions 3.1 and 5.3. Then, for every $w \in Q^b(h)$ and $w_\Gamma \in Q^\Gamma(h)$, it holds*

$$|\mathcal{R}_b(p, w)|^2 \lesssim \sum_{E \in \mathcal{T}_h} \frac{h_E^{2(s_E-1)}}{k_E^{2(r_E-1)}} \|\mathcal{E} p\|_{H^{r_E}(T_E)}^2 \left[\bar{\nu}_E^2 \max_{F \subset \partial E \setminus (\Gamma \cup \partial \Omega_D)} \sigma_F^{-1} \left(\frac{k_E}{h_E} + \frac{k_E^2}{h_E} \right) \right] \cdot \|w\|_{b,DG}^2, \quad (31)$$

$$\begin{aligned} |\mathcal{R}_\Gamma(p_\Gamma, w_\Gamma)|^2 &\lesssim \left(\sum_{F \in \Gamma_h} \frac{h_F^{2(s_F-1)}}{k_F^{2(r_F-1)}} \|\mathcal{E}_\Gamma p_\Gamma\|_{H^{r_F}(T_F)}^2 \left[(\bar{\nu}_F^\tau)^2 \max_{e \subset \partial F \setminus (\mathcal{I} \cap \partial \Gamma_N \cup \partial \Gamma_F)} \sigma_e^{-1} \left(\frac{k_F}{h_F} + \frac{k_F^2}{h_F} \right) \right] \right. \\ &\quad \left. + \sum_{k=1}^{N_\Gamma} \sum_{\substack{F \in \gamma_{h,k} \\ \partial F \cap \mathcal{I} \neq \emptyset}} \frac{h_F^{2(s_F-1)}}{k_F^{2(r_F-1)}} \|\mathcal{E}_{\gamma_k} p_\Gamma^k\|_{H^{r_F}(T_F)}^2 \left[(\bar{\nu}_F^\tau)^2 \max_{e \subset \partial F \cap \mathcal{I}} (\sigma_e^\cap)^{-1} \left(\frac{k_F}{h_F} + \frac{k_F^2}{h_F} \right) \right] \right) \cdot \|w_\Gamma\|_{\Gamma, DG}^2, \end{aligned} \quad (32)$$

where, in (31), the extension operator \mathcal{E} is to be interpreted as \mathcal{E}_j if $E \subset \Omega_j$. Similarly, in (32), \mathcal{E}_Γ is to be interpreted as \mathcal{E}_{γ_k} if $F \subset \gamma_k$.

Proof. Integrating by parts elementwise and using the fact that (p, p_Γ) satisfies (9) and the regularity Assumption 3.1, we obtain the following expression for the residuals

$$\begin{aligned}\mathcal{R}_b(p, w) &= \sum_{F \in \mathcal{F}_h^I \cup \mathcal{F}_h^D} \int_F \{\boldsymbol{\nu}(\nabla p - \mathbf{\Pi}_{\mathbf{W}_h^b}(\nabla p))\} \cdot [w], \\ \mathcal{R}_\Gamma(p_\Gamma, w_\Gamma) &= \sum_{e \in \mathcal{E}_{\Gamma, h}^I \cup \mathcal{E}_{\Gamma, h}^D \cup \mathcal{E}_{\Gamma, h}^\Omega} \int_e \{\boldsymbol{\nu}_\Gamma^\tau \ell_\Gamma(\nabla p_\Gamma - \mathbf{\Pi}_{\mathbf{W}_h^\Gamma}(\nabla p_\Gamma))\} \cdot [w_\Gamma].\end{aligned}$$

For the proof of (31), we refer to [6, 7]. Here, we only focus on the proof of (32). To this aim, we consider the following two terms separately:

$$\begin{aligned}(a) &:= \int_{\mathcal{E}_{\Gamma, h}^I \cup \mathcal{E}_{\Gamma, h}^D} \{\ell_\Gamma \boldsymbol{\nu}_\Gamma^\tau(\nabla p_\Gamma - \mathbf{\Pi}_{\mathbf{W}_h^\Gamma}(\nabla p_\Gamma))\} \cdot [q_\Gamma] \\ (b) &:= \int_{\mathcal{E}_{\Gamma, h}^\Omega} \{\ell_\Gamma \boldsymbol{\nu}_\Gamma^\tau(\nabla p_\Gamma - \mathbf{\Pi}_{\mathbf{W}_h^\Gamma}(\nabla p_\Gamma))\}_\cap \cdot [q_\Gamma]_\cap.\end{aligned}$$

Employing the Cauchy-Schwarz inequality and the definition of norm $\|\cdot\|_{\Gamma, DG}$, we obtain

$$|(a)|^2 \lesssim \left(\int_{\mathcal{E}_{\Gamma, h}^I \cup \mathcal{E}_{\Gamma, h}^D} \sigma_e^{-1} |\{\ell_\Gamma \boldsymbol{\nu}_\Gamma^\tau(\nabla p_\Gamma - \mathbf{\Pi}_{\mathbf{W}_h^\Gamma}(\nabla p_\Gamma))\}|^2 \right) \cdot \|q_\Gamma\|_{\Gamma, DG}^2.$$

Let $\tilde{\Pi}$ denote also the vector-valued generalization of the interpolation operator $\tilde{\Pi}$ defined in 5.2. Then, using triangular inequality we can write

$$\begin{aligned}\sum_{e \in \mathcal{E}_{\Gamma, h}^I \cup \mathcal{E}_{\Gamma, h}^D} \sigma_e^{-1} \int_e |\{\ell_\Gamma \boldsymbol{\nu}_\Gamma^\tau(\nabla p_\Gamma - \mathbf{\Pi}_{\mathbf{W}_h^\Gamma}(\nabla p_\Gamma))\}|^2 &\lesssim \sum_{e \in \mathcal{E}_{\Gamma, h}^I \cup \mathcal{E}_{\Gamma, h}^D} \sigma_e^{-1} \int_e |\{\ell_\Gamma \boldsymbol{\nu}_\Gamma^\tau(\nabla p_\Gamma - \tilde{\Pi}(\nabla p_\Gamma))\}|^2 \\ &+ \sum_{e \in \mathcal{E}_{\Gamma, h}^I \cup \mathcal{E}_{\Gamma, h}^D} \sigma_e^{-1} \int_e |\{\ell_\Gamma \boldsymbol{\nu}_\Gamma^\tau \mathbf{\Pi}_{\mathbf{W}_h^\Gamma}(\nabla p_\Gamma - \tilde{\Pi}(\nabla p_\Gamma))\}|^2 \\ &\equiv (1a) + (2a).\end{aligned}$$

Term (1a) can be bounded, employing the approximation results of Lemma 5.2, as

$$(1a) \lesssim \sum_{F \in \Gamma_h} \frac{h_F^{2(s_F-1)}}{k_F^{2(r_F-1)}} ((\bar{\boldsymbol{\nu}}_F^\tau)^2 \max_{e \subset \partial F \setminus (\mathcal{I}_\Gamma \cup \partial \Gamma_N \cup \partial \Gamma_F)} \sigma_e^{-1} \frac{h_F^{-1}}{k_F^{-1}}) \|\mathcal{E}_\Gamma p_\Gamma\|_{H^{r_F}(T_F)}^2.$$

Exploiting, in order: the boundedness of the permeability tensor $\ell_\Gamma \boldsymbol{\nu}_\Gamma^\tau$, inverse inequality (19), the L^2 -stability of the projector $\mathbf{\Pi}_{\mathbf{W}_h^\Gamma}$ and the approximation results of Lemma 5.2, we can bound term (1b) as:

$$\begin{aligned}(2a) &\lesssim \sum_{F \in \Gamma_h} \max_{e \subset \partial F \setminus (\mathcal{I}_\Gamma \cup \partial \Gamma_N \cup \partial \Gamma_F)} \sigma_e^{-1} (\bar{\boldsymbol{\nu}}_F^\tau)^2 \|\mathbf{\Pi}_{\mathbf{W}_h^\Gamma}(\tilde{\Pi}(\nabla p_\Gamma) - \nabla p_\Gamma)\|_{L^2(\partial F)}^2 \\ &\lesssim \sum_{F \in \Gamma_h} \max_{e \subset \partial F \setminus (\mathcal{I}_\Gamma \cup \partial \Gamma_N \cup \partial \Gamma_F)} \sigma_e^{-1} (\bar{\boldsymbol{\nu}}_F^\tau)^2 \frac{k_F^2}{h_F} \|\tilde{\Pi}(\nabla p_\Gamma) - \nabla p_\Gamma\|_{L^2(F)}^2 \\ &\lesssim \sum_{F \in \Gamma_h} \frac{h_F^{2(s_F-1)}}{k_F^{2(r_F-1)}} \|\mathcal{E}_\Gamma p_\Gamma\|_{H^{r_F}(T_F)}^2 \left((\bar{\boldsymbol{\nu}}_F^\tau)^2 \frac{k_F^2}{h_F} \max_{e \subset \partial F \setminus (\mathcal{I}_\Gamma \cup \partial \Gamma_N \cup \partial \Gamma_F)} \sigma_e^{-1} \right).\end{aligned}$$

Next, we consider term (b). Employing the Cauchy-Schwarz inequality and the definition of the average operator at the intersection $\{\cdot\}_\cap$, we obtain

$$|(b)|^2 \lesssim \left(\sum_{k=1}^{N_\Gamma} \sum_{e \in \mathcal{E}_{\gamma_k, h}^\cap} \int_e (\sigma_e^\cap)^{-1} |\ell_\Gamma \boldsymbol{\nu}_\Gamma^\tau (\nabla p_\Gamma^k - \mathbf{\Pi}_{\mathbf{W}_h^{\gamma_k}} (\nabla p_\Gamma))|^2 \right) \cdot \|q_\Gamma\|_{\Gamma, DG}^2.$$

Recalling that $\tilde{\Pi}$ denotes the vector-valued generalization of the interpolation operator of Lemma 5.2, we can write

$$\begin{aligned} & \sum_{k=1}^{N_\Gamma} \sum_{e \in \mathcal{E}_{\gamma_k, h}^\cap} \int_e (\sigma_e^\cap)^{-1} |\ell_k \boldsymbol{\nu}_{\gamma_k}^\tau (\nabla p_\Gamma^k - \mathbf{\Pi}_{\mathbf{W}_h^{\gamma_k}} (\nabla p_\Gamma))|^2 \\ & \lesssim \sum_{k=1}^{N_\Gamma} \sum_{e \in \mathcal{E}_{\gamma_k, h}^\cap} \left(\int_e (\sigma_e^\cap)^{-1} |\ell_k \boldsymbol{\nu}_{\gamma_k}^\tau (\nabla p_\Gamma^k - \tilde{\Pi}(\nabla p_\Gamma^k))|^2 + \int_e (\sigma_e^\cap)^{-1} |\ell_k \boldsymbol{\nu}_{\gamma_k}^\tau \mathbf{\Pi}_{\mathbf{W}_h^{\gamma_k}} (\nabla p_\Gamma^k - \tilde{\Pi}(\nabla p_\Gamma^k))|^2 \right) \\ & \equiv (1b) + (2b). \end{aligned}$$

Employing arguments analogous to those for bounding terms (1a) and (2a), we can then write

$$(1b) \lesssim \sum_{k=1}^{N_\Gamma} \sum_{\substack{F \in \gamma_{h,k} \\ \partial F \cap \mathcal{I}_\cap \neq \emptyset}} \frac{h_F^{2(s_F-1)}}{k_F^{2(r_F-1)}} \left((\bar{\boldsymbol{\nu}}_F^\tau)^2 \max_{e \subset \partial F \cap \mathcal{I}_\cap} (\sigma_e^\cap)^{-1} \frac{h_F^{-1}}{k_F^{-1}} \right) \|\mathcal{E}_{\gamma_k} p_\Gamma^k\|_{H^{r_F}(T_F)}^2,$$

and

$$\begin{aligned} (2b) & \lesssim \sum_{k=1}^{N_\Gamma} \sum_{\substack{F \in \gamma_{h,k} \\ \partial F \cap \mathcal{I}_\cap \neq \emptyset}} \max_{e \subset \partial F \cap \mathcal{I}_\cap} (\sigma_e^\cap)^{-1} (\bar{\boldsymbol{\nu}}_F^\tau)^2 \|\mathbf{\Pi}_{\mathbf{W}_h^\cap} (\tilde{\Pi}(\nabla p_\Gamma^k) - \nabla p_\Gamma^k)\|_{L^2(\partial F)}^2 \\ & \lesssim \sum_{k=1}^{N_\Gamma} \sum_{\substack{F \in \gamma_{h,k} \\ \partial F \cap \mathcal{I}_\cap \neq \emptyset}} \max_{e \subset \partial F \cap \mathcal{I}_\cap} (\sigma_e^\cap)^{-1} (\bar{\boldsymbol{\nu}}_F^\tau)^2 \frac{k_F^2}{h_F} \|\tilde{\Pi}(\nabla p_\Gamma^k) - \nabla p_\Gamma^k\|_{L^2(F)}^2 \\ & \lesssim \sum_{k=1}^{N_\Gamma} \sum_{\substack{F \in \gamma_{h,k} \\ \partial F \cap \mathcal{I}_\cap \neq \emptyset}} \frac{h_F^{2(s_F-1)}}{k_F^{2(r_F-1)}} \|\mathcal{E}_{\gamma_k} p_\Gamma^k\|_{H^{r_F}(T_F)}^2 \left((\bar{\boldsymbol{\nu}}_F^\tau)^2 \frac{k_F^2}{h_F} \max_{e \subset \partial F \cap \mathcal{I}_\cap} (\sigma_e^\cap)^{-1} \right). \end{aligned}$$

This concludes the proof. \square

Theorem 5.6. *Let $\mathcal{T}_\# = \{T_E\}$ and $\mathcal{F}_\# = \{T_F\}$ denote the associated coverings of Ω and Γ , respectively, consisting of shape-regular simplexes as in Definition 5.1, satisfying Assumptions 5.1. Let (p, p_Γ) be the solution of problem (9) and $(p_h, p_{\Gamma, h}) \in Q_h^b \times Q_h^\Gamma$ be its approximation obtained with the method (18), with the penalization parameters given by (20) and (21) and*

σ_0 and $\sigma_{0,\Gamma}$ sufficiently large. Moreover, suppose that the exact solution (p, p_Γ) satisfies the regularity Assumptions 3.1 and 5.3. Then, the following error bound holds:

$$\begin{aligned} \|(p, p_\Gamma) - (p_h, p_{\Gamma,h})\|^2 &\lesssim \sum_{E \in \mathcal{T}_h} \frac{h_E^{2(s_E-1)}}{k_E^{2(r_E-1)}} G_E(h_E, k_E, \bar{\nu}_E) \|\mathcal{E}p\|_{H^{r_E}(T_E)}^2 \\ &\quad + \sum_{F \in \Gamma_h} \frac{h_F^{2(s_F-1)}}{k_F^{2(r_F-1)}} G_F(h_F, k_F, \bar{\nu}_F^\tau) \|\mathcal{E}_\Gamma p_\Gamma\|_{H^{r_F}(T_F)}^2 \\ &\quad + \sum_{k=1}^{N_\Gamma} \sum_{\substack{F \in \gamma_{h,k} \\ \partial F \cap \mathcal{I}_\Gamma \neq \emptyset}} \frac{h_F^{2(s_F-1)}}{k_F^{2(r_F-1)}} G_F^\cap(h_F, k_F, \bar{\nu}_F^\tau) \|\mathcal{E}_{\gamma_k} p_\Gamma^k\|_{H^{r_F}(T_F)}^2, \end{aligned}$$

where the $\mathcal{E}p$ is to be interpreted as $\mathcal{E}_j p_j$ when $E \subset \Omega_j$, $j = 1, \dots, N_\omega$, and $\mathcal{E}_\Gamma p_\Gamma$ is to be interpreted as $\mathcal{E}_{\gamma_k} p_\Gamma^k$ when $F \subset \gamma_k$, $k = 1, \dots, N_\Gamma$. Here, $s_E = \min(k_E + 1, r_E)$ and $s_F = \min(k_F + 1, r_F)$ and for every $E \in \mathcal{T}_h$ and $F \in \Gamma_h$, the constants G_E , G_F and G_F^\cap are defined as:

$$\begin{aligned} G_E(h_E, k_E, \bar{\nu}_E) &= \bar{\nu}_E + h_E k_E^{-1} \max_{F \subset \partial E \setminus \Gamma} \sigma_F + (\alpha_\Gamma + \beta_\Gamma) h_E k_E^{-1} \\ &\quad + \bar{\nu}_E^2 h_E^{-1} k_E \max_{F \subset \partial E \setminus \Gamma} \sigma_F^{-1} + \bar{\nu}_E^2 h_E^{-1} k_E^2 \max_{F \subset \partial E \setminus \Gamma} \sigma_F^{-1}, \\ G_F(h_F, k_F, \bar{\nu}_F^\tau) &= \bar{\nu}_F^\tau + h_F k_F^{-1} \max_{e \subset \partial F \setminus (\mathcal{I}_\Gamma \cup \partial \Gamma_N \cup \partial \Gamma_F)} \sigma_e + \alpha_\Gamma h_F^2 k_F^{-2} \\ &\quad + (\bar{\nu}_F^\tau)^2 h_F^{-1} k_F \max_{e \subset \partial F \setminus (\mathcal{I}_\Gamma \cup \partial \Gamma_N \cup \partial \Gamma_F)} \sigma_e^{-1} + (\bar{\nu}_F^\tau)^2 h_F^{-1} k_F^2 \max_{e \subset \partial F \setminus (\mathcal{I}_\Gamma \cup \partial \Gamma_N \cup \partial \Gamma_F)} \sigma_e^{-1} \\ G_F^\cap(h_F, k_F, \bar{\nu}_F^\tau) &= h_F k_F^{-1} \max_{e \subset \partial F \cap \mathcal{I}_\Gamma} \sigma_e^\cap \\ &\quad + (\bar{\nu}_F^\tau)^2 h_F^{-1} k_F \max_{e \subset \partial F \cap \mathcal{I}_\Gamma} (\sigma_e^\cap)^{-1} + (\bar{\nu}_F^\tau)^2 h_F^{-1} k_F^2 \max_{e \subset \partial F \cap \mathcal{I}_\Gamma} (\sigma_e^\cap)^{-1}. \end{aligned}$$

Proof. From Lemma 5.4 we know that the error satisfies the following bound

$$\begin{aligned} \|(p, p_\Gamma) - (p_h, p_{\Gamma,h})\| &\lesssim \underbrace{\inf_{(q, q_\Gamma) \in Q_h^b \times Q_\Gamma^b} \|(p, p_\Gamma) - (q, q_\Gamma)\|}_I \\ &\quad + \underbrace{\sup_{(w, w_\Gamma) \in Q_h^b \times Q_\Gamma^b} \frac{|\mathcal{R}_h((p, p_\Gamma), (w, w_\Gamma))|}{\|(w, w_\Gamma)\|}}_{II}. \end{aligned} \quad (33)$$

We estimate the two terms on the right-hand side of (33) separately. We can rewrite term I as

$$\begin{aligned} I &= \inf_{(q, q_\Gamma) \in Q_h^b \times Q_\Gamma^b} \left(\|p - q\|_{b,DG}^2 + \|p_\Gamma - q_\Gamma\|_{\Gamma,DG}^2 + \|(p - q, p_\Gamma - q_\Gamma)\|_{\mathcal{C}}^2 \right) \\ &\leq \underbrace{\|p - \tilde{\Pi}p\|_{b,DG}^2}_{(a)} + \underbrace{\|p_\Gamma - \tilde{\Pi}p_\Gamma\|_{\Gamma,DG}^2}_{(b)} + \underbrace{\|(p - \tilde{\Pi}p, p_\Gamma - \tilde{\Pi}p_\Gamma)\|_{\mathcal{C}}^2}_{(c)}. \end{aligned}$$

We consider each of the three terms separately. To bound term (a), we exploit the two approximation results stated in Lemma 5.2; we obtain that

$$\begin{aligned}
(a) &\leq \|p - \tilde{\Pi}p\|_{b,DG}^2 = \sum_{E \in \mathcal{T}_h} \|\nu^{1/2} \nabla(p - \tilde{\Pi}p)\|_{L^2(E)}^2 + \sum_{F \in \mathcal{F}_h^I \cup \mathcal{F}_h^D} \sigma_F \|\llbracket p - \tilde{\Pi}p \rrbracket\|_{L^2(F)}^2 \\
&\lesssim \sum_{E \in \mathcal{T}_h} \left[\bar{\nu}_E |p - \tilde{\Pi}p|_{H^1(E)}^2 + \left(\max_{F \subset \partial E \setminus (\Gamma \cup \partial \Omega_N)} \sigma_F \right) \|p - \tilde{\Pi}p\|_{L^2(\partial E)}^2 \right] \\
&\lesssim \sum_{E \in \mathcal{T}_h} \left[\frac{h_E^{2(s_E-1)}}{k_E^{2(r_E-1)}} \bar{\nu}_E \|\mathcal{E}p\|_{H^{r_E}(T_E)}^2 + \frac{h_E^{2(s_E-1/2)}}{k_E^{2(r_E-1/2)}} \left(\max_{F \subset \partial E \setminus (\Gamma \cup \partial \Omega_N)} \sigma_F \right) \|\mathcal{E}p\|_{H^{r_E}(T_E)}^2 \right] \\
&= \sum_{E \in \mathcal{T}_h} \frac{h_E^{2(s_E-1)}}{k_E^{2(r_E-1)}} \|\mathcal{E}p\|_{H^{r_E}(T_E)}^2 \left(\bar{\nu}_E + \frac{h_E}{k_E} \left(\max_{F \subset \partial E \setminus (\Gamma \cup \partial \Omega_N)} \sigma_F \right) \right).
\end{aligned}$$

Using analogous interpolation estimates on the fracture we can bound term (b) as follows:

$$\begin{aligned}
(b) &\leq \|p_\Gamma - \tilde{\Pi}p_\Gamma\|_{\Gamma,DG}^2 \lesssim \sum_{F \in \Gamma_h} \|\nu_\Gamma^\tau \ell_\Gamma \nabla(p_\Gamma - \tilde{\Pi}p_\Gamma)\|_{L^2(F)}^2 + \sum_{e \in \mathcal{E}_{\Gamma,h}^I \cup \mathcal{E}_{\Gamma,h}^D \cup \mathcal{E}_{\Gamma,h}^\cap} \sigma_e \|\llbracket p_\Gamma - \tilde{\Pi}p_\Gamma \rrbracket\|_{L^2(e)}^2 \\
&\lesssim \sum_{F \in \Gamma_h} \frac{h_F^{2(s_F-1)}}{k_F^{2(r_F-1)}} \|\mathcal{E}_\Gamma p_\Gamma\|_{H^{r_F}(T_F)}^2 \left(\bar{\nu}_F^\tau + \frac{h_F}{k_F} \max_{e \subseteq \partial F \setminus (\mathcal{I}_\cap \cup \partial \Gamma_N \cup \partial \Gamma_F)} \sigma_e \right) \\
&\quad + \sum_{k=1}^{N_\Gamma} \sum_{\substack{F \in \gamma_{h,k} \\ \partial F \cap \mathcal{I}_\cap \neq \emptyset}} \frac{h_F^{2(s_F-1)}}{k_F^{2(r_F-1)}} \|\mathcal{E}_{\gamma_k} p_\Gamma^k\|_{H^{r_F}(T_F)}^2 \left(\frac{h_F}{k_F} \max_{e \subseteq \partial F \cap \mathcal{I}_\cap} \sigma_e^\cap \right).
\end{aligned}$$

Finally, for term (c), we have

$$\begin{aligned}
(c) &\leq \|(p - \tilde{\Pi}p, p_\Gamma - \tilde{\Pi}p_\Gamma)\|_{\mathcal{C}}^2 \leq \beta_\Gamma \sum_{F \in \Gamma_h} \|\llbracket p - \tilde{\Pi}p \rrbracket\|_{L^2(F)}^2 + \alpha_\Gamma \sum_{F \in \Gamma_h} \|\{p - \tilde{\Pi}p\}\|_{L^2(F)}^2 \\
&\quad + \alpha_\Gamma \sum_{F \in \Gamma_h} \|p_\Gamma - \tilde{\Pi}p_\Gamma\|_{L^2(F)}^2.
\end{aligned}$$

Exploiting the interpolation result (29), we deduce that

$$\begin{aligned}
\beta_\Gamma \sum_{F \in \Gamma_h} \|\llbracket p - \tilde{\Pi}p \rrbracket\|_{L^2(F)}^2 &\leq \beta_\Gamma \sum_{\substack{E \in \mathcal{T}_h \\ \partial E \cap \Gamma \neq \emptyset}} \|p - \tilde{\Pi}p\|_{L^2(\partial E)}^2 \lesssim \beta_\Gamma \sum_{\substack{E \in \mathcal{T}_h \\ \partial E \cap \Gamma \neq \emptyset}} \frac{h_E^{2(s_E-1/2)}}{k_E^{2(r_E-1/2)}} \|\mathcal{E}p\|_{H^{r_E}(T_E)}^2 \\
&= \beta_\Gamma \sum_{\substack{E \in \mathcal{T}_h \\ \partial E \cap \Gamma \neq \emptyset}} \frac{h_E^{2(s_E-1)}}{k_E^{2(r_E-1)}} \|\mathcal{E}p\|_{H^{r_E}(T_E)}^2 \frac{h_E}{k_E}.
\end{aligned}$$

Similarly, we have

$$\alpha_\Gamma \sum_{F \in \Gamma_h} \|\{p - \tilde{\Pi}p\}\|_{L^2(F)}^2 \lesssim \alpha_\Gamma \sum_{\substack{E \in \mathcal{T}_h \\ \partial E \cap \Gamma \neq \emptyset}} \frac{h_E^{2(s_E-1)}}{k_E^{2(r_E-1)}} \|\mathcal{E}p\|_{H^{r_E}(T_E)}^2 \frac{h_E}{k_E}.$$

Moreover, using interpolation estimates for the fracture network, we obtain

$$\begin{aligned} \alpha_\Gamma \sum_{F \in \Gamma_h} \|p_\Gamma - \tilde{\Pi} p_\Gamma\|_{L^2(F)}^2 &\lesssim \alpha_\Gamma \sum_{F \in \Gamma_h} \frac{h_F^{2s_F}}{k_F^{2r_F}} \|\mathcal{E} p_\Gamma\|_{H^{r_F}(T_F)}^2 \\ &= \alpha_\Gamma \sum_{F \in \Gamma_h} \frac{h_F^{2(s_F-1)}}{k_F^{2(r_F-1)}} \|\mathcal{E} p_\Gamma\|_{H^{r_F}(T_F)}^2 \frac{h_F^2}{k_F^2}. \end{aligned}$$

Combining all the previous estimates, we can bound term I on the right-hand side of (33) as follows:

$$\begin{aligned} I &\lesssim \frac{h_E^{2(s_E-1)}}{k_E^{2(r_E-1)}} \|\mathcal{E} p\|_{H^{r_E}(T_E)}^2 \left[\bar{\nu}_E + \frac{h_E}{k_E} \max_{F \subset \partial E \setminus (\Gamma \cup \partial \Omega_N)} \sigma_F + (\alpha_\Gamma + \beta_\Gamma) \frac{h_E}{k_E} \right] \\ &\quad + \sum_{F \in \Gamma_h} \frac{h_F^{2(s_F-1)}}{k_F^{2(r_F-1)}} \|\mathcal{E}_\Gamma p_\Gamma\|_{H^{r_F}(T_F)}^2 \left[\bar{\nu}_F^\tau + \frac{h_F}{k_F} \max_{e \subseteq \partial F \setminus (\mathcal{I}_\Gamma \cup \partial \Gamma_N \cup \partial \Gamma_F)} \sigma_e + \alpha_\Gamma \frac{h_F^2}{k_F^2} \right] \\ &\quad + \sum_{k=1}^{N_\Gamma} \sum_{\substack{F \in \gamma_{h,k} \\ \partial F \cap \mathcal{I}_\Gamma \neq \emptyset}} \frac{h_F^{2(s_F-1)}}{k_F^{2(r_F-1)}} \|\mathcal{E}_{\gamma_k} p_\Gamma^k\|_{H^{r_F}(T_F)}^2 \left[\frac{h_F}{k_F} \max_{e \subseteq \partial F \cap \mathcal{I}_\Gamma} \sigma_e^\cap \right]. \quad (34) \end{aligned}$$

Finally, the desired estimate follows from the combination of (34), together with the bound on Term II that derives from what observed in (30) and Lemma 5.5. \square

6 Numerical experiments

In this section we present several numerical examples, with increasing complexity, in order to validate the performance of our method. In the experiments the analytical solution is known, so that we are able to verify the convergence rates obtained in Theorem 5.6. We point out that choice of the model coefficients is here made only with the aim of testing the effectiveness of the numerical method and it does not intend to have any physical meaning. We remark that, in all the presented test cases, the pressure continuity condition at the intersection points (8a) is satisfied, however in some of them the no flux condition (8b) does not hold. To take this into account, we need to modify formulation (18), adding on the right hand side the term

$$\int_{\mathcal{E}_{\Gamma,h}^\cap} \llbracket \boldsymbol{\nu}_\Gamma^\tau \ell_\Gamma \nabla_\tau p_\Gamma \rrbracket_\cap \{q_\Gamma\}_\cap, \quad (35)$$

where the quantity $\llbracket \boldsymbol{\nu}_\Gamma^\tau \ell_\Gamma \nabla_\tau p_\Gamma \rrbracket_\cap = \sum_{k=1}^{N_\Gamma} \boldsymbol{\nu}_{\gamma_k}^\tau \ell_k \nabla_\tau p_\Gamma^k \cdot \boldsymbol{\tau}_k$ is given.

For all the experiments we choose quadratic polynomial degree for both the bulk and fracture problems. Moreover, we always choose the permeability tensor in the bulk $\boldsymbol{\nu} = \mathbf{I}$, so as to focus mainly on the fracture problem. All the numerical tests have been implemented in MATLAB[®] and employ polygonal grids.

6.1 Example 1: Vertical fracture

As first test case, we modify a test case presented in [6], splitting the single fracture in 3 parts. In particular, we consider the domain $\Omega = (0,1)^2$ and the fracture network composed of the fractures $\gamma_1 = \{(x,y) \in \Omega : x = 0.5, 0 < y < 0.5\}$, $\gamma_2 = \{(x,y) \in \Omega : x = 0.5, 0.5 < y < 0.75\}$ and $\gamma_3 = \{(x,y) \in \Omega : x = 0.5, 0.75 < y < 1\}$, see Figure 5(a). Note that both the tips of the fracture γ_2 are intersection tips.

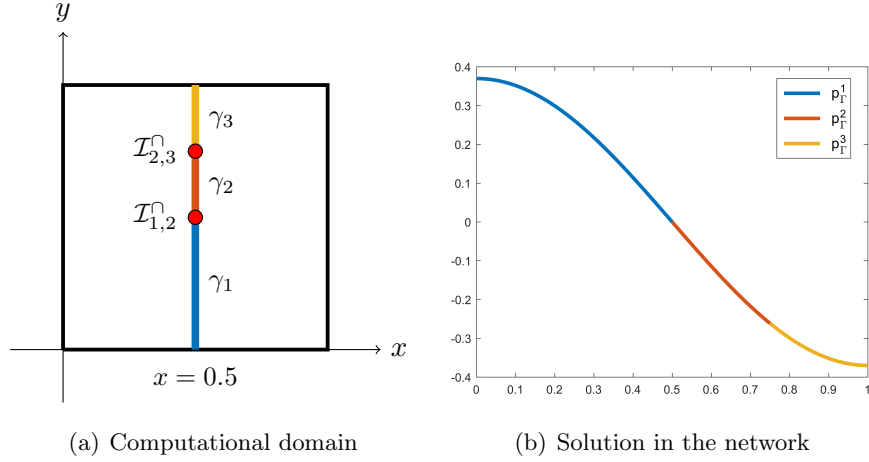


Figure 5: Example 1: Computational domain (left) and computed fracture pressures (right).

We choose the exact solutions in the bulk and in the fractures as follows

$$p = \begin{cases} \sin(4x) \cos(\pi y) & \text{if } x < 0.5, \\ \cos(4x) \cos(\pi y) & \text{if } x > 0.5, \end{cases} \quad p_{\Gamma}^k = \xi[\cos(2) + \sin(2)] \cos(\pi y), \quad k = 1, 2, 3$$

so that they satisfy the coupling conditions (6) with $\boldsymbol{\nu} = \mathbf{I}$, provided that, $\forall k = 1, 2, 3$, we choose $\beta_{\gamma_k} = 2$ that is $\boldsymbol{\nu}_{\gamma_k}^n / \ell_k = 4$. We impose Dirichlet boundary conditions on the whole $\partial\Omega$ and also on $\partial\Gamma$. Finally, the source term in the bulk is chosen accordingly as

$$f = \begin{cases} \sin(4x) \cos(\pi y)(16 + \pi^2) & \text{if } x < 0.5, \\ \cos(4x) \cos(\pi y)(16 + \pi^2) & \text{if } x > 0.5, \end{cases}$$

and, given $\forall k = 1, 2, 3$ the values $\boldsymbol{\nu}_{\gamma_k}^{\tau}$ of the tangential components of the permeability tensor in the fracture, the fracture forcing terms are set as

$$f_{\Gamma}^k = \cos(\pi y)[\cos(2) + \sin(2)](\xi \boldsymbol{\nu}_{\gamma_k}^{\tau} \pi^2 + \frac{4}{\ell_k}).$$

Clearly, pressure continuity at the intersection point (8a) is satisfied regardless of the values chosen for the fracture coefficients $\boldsymbol{\nu}_{\Gamma}^{\tau}$, ν_{Γ}^n and ℓ_{Γ} . However, flux conservation (8b) does not

hold if the values vary from fracture to fracture. For this reason, we need to modify the right hand side of the formulation as in (35).

We perform two simulations, varying the values of the fracture coefficients (always satisfying the constraint $\beta_\Gamma = 2$). In particular, we take

- Case (a):

$$\begin{aligned} \boldsymbol{\nu}_\Gamma^\tau &= [3 \cdot 10^4 \quad 2 \cdot 10^3 \quad 4 \cdot 10^4], \\ \boldsymbol{\nu}_\Gamma^n &= 4 * [10^{-4} \quad 10^{-2} \quad 10^{-5}], \\ \ell_\Gamma &= [10^{-4} \quad 10^{-2} \quad 10^{-5}]; \end{aligned} \tag{36}$$

- Case (b):

$$\begin{aligned} \boldsymbol{\nu}_\Gamma^\tau &= [3 \cdot 10^{-4} \quad 2 \cdot 10^{-3} \quad 4 \cdot 10^{-4}], \\ \boldsymbol{\nu}_\Gamma^n &= [10^4 \quad 10^2 \quad 10^5], \\ \ell_\Gamma &= 0.25 * [10^4 \quad 10^2 \quad 10^5]; \end{aligned} \tag{37}$$

Finally, in all the experiments we set $\xi = 0.75$.

In Figure 5(b) we show the numerical solution for the problem in the fracture network for case (a), where one can clearly see that the continuity condition at the intersection points (8a) is satisfied. In Figures 6(a)-6(b) we report the computed errors $\|p - p_h\|_{b,DG}$ (loglog scale) for the bulk problem as a function of the inverse of the mesh size $1/h$ and the corresponding computed errors $\|p_\Gamma - p_{\Gamma,h}\|_{\Gamma,DG}$ (loglog scale) in the fracture network. We recall that we are taking the polynomial degree $k = 2$ for both the bulk and fracture problems. On the left we show the results obtained for test case (a) (with coefficients as in (36)), while on the right, we report the results for the case (b) (with coefficient as in (37)). As predicted from our theoretical error bounds, a convergence of order 2 is clearly observed for both $\|p - p_h\|_{b,DG}$ and $\|p_\Gamma - p_{\Gamma,h}\|_{\Gamma,DG}$. Moreover, the convergence is improved of one order if we consider the errors in the L^2 -norms $\|p - p_h\|_{L^2(\Omega)}$ and $\|p_\Gamma - p_{\Gamma,h}\|_{L^2(\Gamma)}$.

6.2 Example 2: Y-shaped intersection

In the second test case we take the bulk $\Omega = (-2, 2)^2$ and the fracture network Γ consisting of the fractures $\gamma_1 = \{(x, y) \in \Omega : x = y, -2 < y < 0\}$, $\gamma_2 = \{(x, y) \in \Omega : x = y, 0 < y < 2\}$ and $\gamma_3 = \{(x, y) \in \Omega : x = 0, 0 < y < 2\}$, see Figure 7. We choose the exact solution in the whole bulk as $p(x, y) = \cos(xy - x^2)$ and the permeability tensor $\boldsymbol{\nu} = \mathbf{I}$. Note that, even if the bulk solution is continuous across the fractures, the first coupling condition in (6) is satisfied because $\nabla p|_\Gamma = \mathbf{0}$. In order for the second coupling condition to hold, we need to choose the solution in the fractures

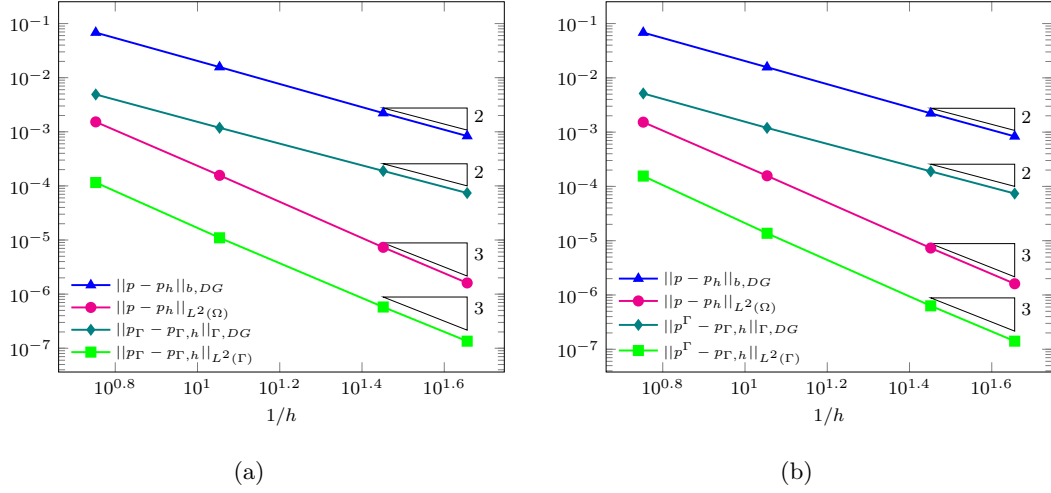


Figure 6: Example 1: Computed errors in the bulk and in the fractures as a function of the inverse of the mesh size (loglog scale). Case (a) on the left and case (b) on the right.

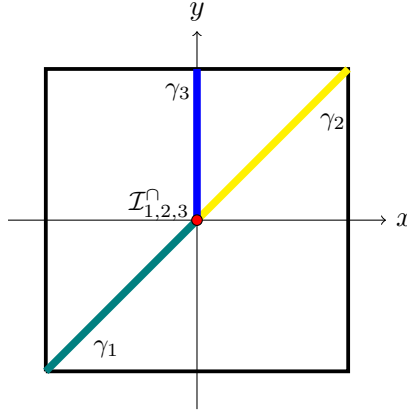


Figure 7: Example 2: computational domain.

$p_\Gamma^k = p|_{\Gamma_k}$ for all $k = 1, 2, 3$, that is $p_\Gamma^k = 1$. Note also that this configuration satisfies the conditions at the intersection (8) irrespective of the choice of the model coefficients. Finally, the source terms are chosen accordingly as $f = \cos(xy - x^2)(y^2 + 5x^2 - 4xy) - 2\sin(xy - x^2)$ and $f_\Gamma = \mathbf{0}$. We impose Dirichlet boundary conditions on the whole $\partial\Omega$ and also on $\partial\Gamma$. In the numerical experiments we choose $\xi = 0.55$.

We perform two simulations, taking the physical parameters in the fracture network as in the previous example, that is for case (a) we choose the coefficients as in (36), while for case (b) as in (37).

Figures 8(a)-8(b) show the computed errors (in loglog scale) $\|p - p_h\|_{b,DG}$ and $\|p_\Gamma - p_{\Gamma,h}\|_{\Gamma,DG}$ for the bulk and fracture problem, respectively (case (a) on the left and case (b) on the right). Also in this case the theoretical convergence rates are achieved and

one order is gained for the L^2 -norm.

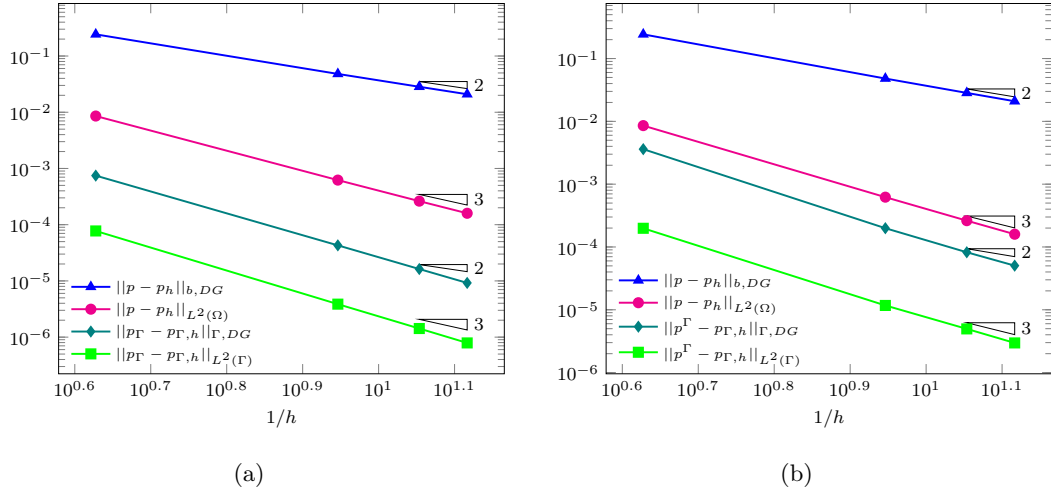


Figure 8: Example 2: Computed errors in the bulk and in the fractures as a function of the inverse of the mesh size (loglog scale). Case (a) on the left and case (b) on the right.

6.3 Example 3: Checkerboard

In the third test case we consider a cross-shaped network of fractures cutting the bulk $\Omega = (-1, 1)^2$. The fractures are defined as $\gamma_1 = \{(x, y) \in \Omega : y = 0, -1 < x < -0.5\}$, $\gamma_2 = \{(x, y) \in \Omega : y = 0, -0.5 < x < 0\}$, $\gamma_3 = \{(x, y) \in \Omega : x = 0, -1 < y < 0\}$, $\gamma_4 = \{(x, y) \in \Omega : y = 0, 0 < x < 1\}$ and $\gamma_5 = \{(x, y) \in \Omega : x = 0, 0 < y < 1\}$, see Figure 9(a). Note that fracture γ_2 presents two intersection tips.

We choose again a solution in the bulk continuous across the fractures $p(x, y) = \cos(\pi x) \cos(\pi y)$ and the permeability tensor $\boldsymbol{\nu} = \mathbf{I}$. In this case, the first coupling condition in (6) is satisfied because $\nabla p|_\Gamma \cdot \mathbf{n}_\Gamma = 0$, where $\mathbf{n}_1 = \mathbf{n}_2 = \mathbf{n}_4 = (0, 1)^T$ and $\mathbf{n}_3 = \mathbf{n}_5 = (1, 0)^T$. The validity of the second coupling condition is satisfied if $p_\Gamma^k = p|_{\Gamma_k}$ for all $k = 1, 2, 3, 4, 5$, that is $p_\Gamma^1 = p_\Gamma^2 = p_\Gamma^4 = \cos(\pi x)$ and $p_\Gamma^3 = p_\Gamma^5 = \cos(\pi y)$.

In the bulk, we impose Neumann boundary conditions on $\partial\Omega_N = \{(x, y) \in \Omega : x = 1\}$ and Dirichlet boundary conditions on the rest of the boundary. Accordingly, at the boundary tips of fractures γ_1 , γ_3 and γ_5 we impose Dirichlet conditions, and at the boundary tip of γ_4 we impose Neumann conditions. In the numerical experiments we choose $\xi = 0.55$. Finally, the source term in the bulk is chosen accordingly as $f = 2\pi^2 \cos(\pi x) \cos(\pi y)$ and, given the physical coefficients $\boldsymbol{\nu}_{\Gamma_k}^\tau$ and ℓ_k , for $k = 1, 2, 3, 4, 5$, the source term for each fracture is $f_\Gamma^k = \pi^2 \cos(\pi x) \boldsymbol{\nu}_{\Gamma_k}^\tau$. Note that, at intersection $\mathcal{I}_{1,2}^\cap$ flux conservation does not hold if the values of the coefficients vary from γ_1 to γ_2 , while at intersection $\mathcal{I}_{2,3,4,5}^\cap$ flux

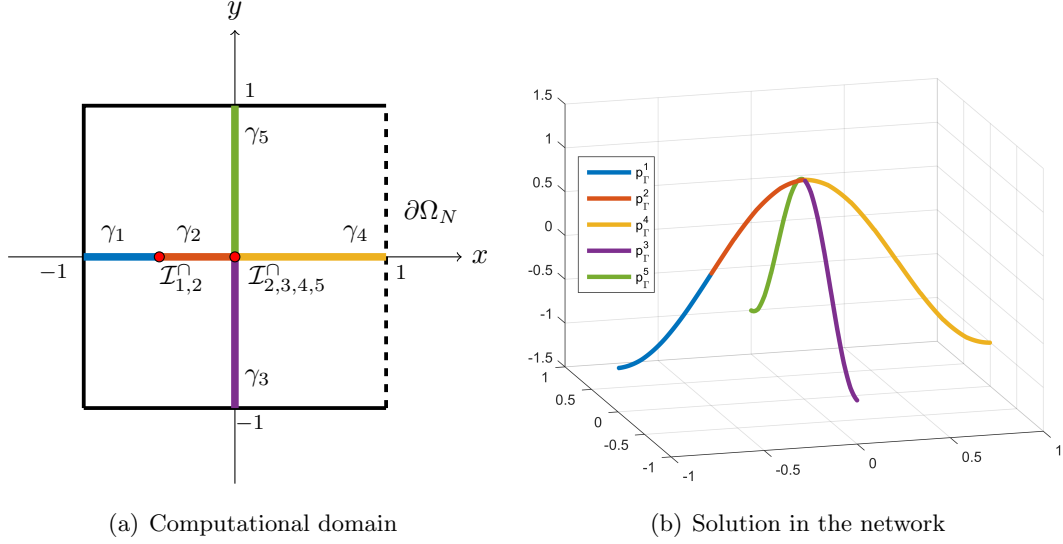


Figure 9: Example 3: Computational domain (left) and computed fracture pressures plotted as 3d-lines (right).

conservation is satisfied for every choice, due to the fact that $\nabla p_{\Gamma}^k|_{\mathcal{I}_{2,3,4,5}^{\cap}} = 0$, for $k = 2, 3, 4, 5$.

We perform two simulations:

- in case (a) we take $\ell_k = \nu_{\gamma_k}^{\tau} = \nu_{\gamma_k}^n = k \cdot 10^k$, for $k = 1, 2, 3, 4, 5$;
- in case (b) we take $\ell_k = \nu_{\gamma_k}^{\tau} = \nu_{\gamma_k}^n = k \cdot 10^{-k}$, for $k = 1, 2, 3, 4, 5$.

In Figure 9(b) we show the numerical solution for the fracture network problem computed with the coefficients of case (a). The values of the fracture pressures are displayed as lines in the 3d space, so that pressure continuity at the intersection points is evident. The plots in Figures 10(a)-10(b) show the computed errors in loglog scale for the bulk and network problems, together with the expected convergence rates. Test case (a) is on the left and test case (b) is on the right. Once again the results are in agreement with the theoretical estimates.

6.4 Example 4: Cross-shaped intersection

We consider the domain $\Omega = (0, 1)^2$ cut by a cross-shaped network made up of the four fractures $\gamma_1 = \{(x, y) \in \Omega : y = 0.5, 0 < x < 0.5\}$, $\gamma_2 = \{(x, y) \in \Omega : x = 0.5, 0 < y < 0.5\}$, $\gamma_3 = \{(x, y) \in \Omega : y = 0.5, 0.5 < x < 1\}$ and $\gamma_4 = \{(x, y) \in \Omega : x = 0.5, 0.5 < y < 1\}$.

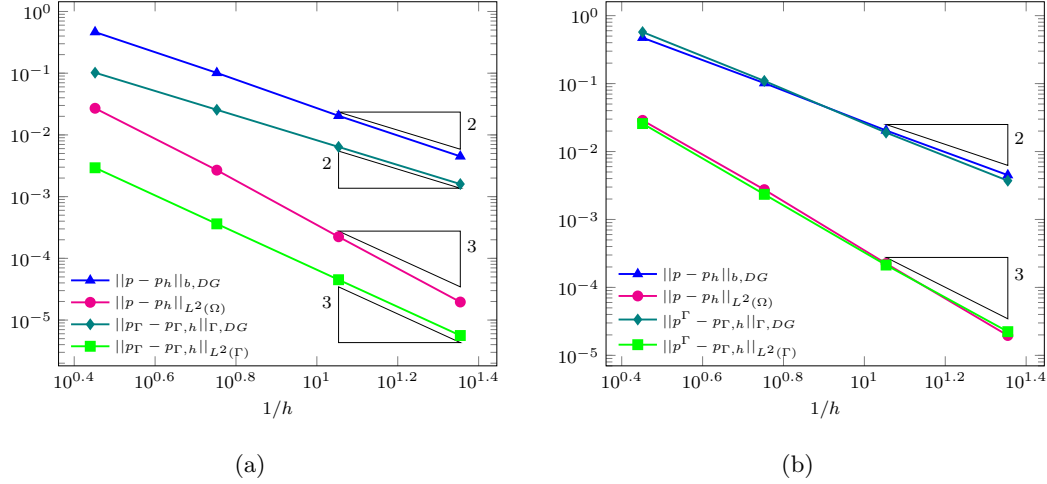


Figure 10: Example 3: Computed errors in the bulk and in the fractures as a function of the inverse of the mesh size (loglog scale). Case (a) on the left and case (b) on the right.

The bulk domain Ω is then subdivided into the sets

$$\begin{aligned}\Omega_A &= \{(x, y) \in \Omega : 0 < x < 0.5, 0 < y < 0.5\}, \\ \Omega_B &= \{(x, y) \in \Omega : 0.5 < x < 1, 0 < y < 0.5\}, \\ \Omega_C &= \{(x, y) \in \Omega : 0.5 < x < 1, 0.5 < y < 1\}, \\ \Omega_D &= \{(x, y) \in \Omega : 0 < x < 0.5, 0.5 < y < 1\},\end{aligned}$$

as shown in Figure 11.

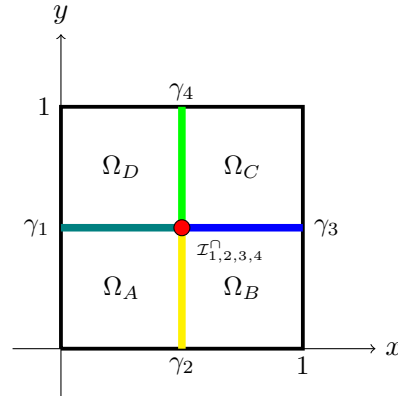


Figure 11: Example 4: computational domain.

In order to define the exact solution for the bulk problem, we introduce the functions

$$\begin{aligned} p_l &= \sin\left(\frac{\pi}{2}x\right) \cos(2\pi y), \\ p_r &= \cos\left(\frac{\pi}{2}x\right) \cos(2\pi y), \\ p_u &= \cos\left(\frac{\pi}{2}y\right) \cos(2\pi x), \\ p_d &= \sin\left(\frac{\pi}{2}y\right) \cos(2\pi x), \end{aligned}$$

where the subscript is related to the position (left, right, up, down). The bulk pressure is then defined in each subdomain of Ω as

$$p(x, y) = \begin{cases} p_l + p_d & \text{in } \Omega_A, \\ p_r + p_d & \text{in } \Omega_B, \\ p_r + p_u & \text{in } \Omega_C, \\ p_l + p_u & \text{in } \Omega_D. \end{cases}$$

If we choose the permeability tensor $\boldsymbol{\nu} = \mathbf{I}$, the bulk source term will have the following expression $f(x, y) = \frac{17}{4}\pi^2 p(x, y)$. Simple calculations show that $p(x, y)$ satisfies the first coupling condition in (6) provided that for $k = 1, 2, 3, 4$, we choose $\beta_{\gamma_k} = \frac{\pi}{4}$, that is $\boldsymbol{\nu}_{\gamma_k}^n = \frac{\pi}{2}\ell_k$. From the second coupling condition we deduce the following expressions for the solutions in the fractures

$$\begin{aligned} p_\Gamma^1 &= \xi\sqrt{2} \cos(2\pi x) - \sin\left(\frac{\pi}{2}x\right), & p_\Gamma^2 &= \xi\sqrt{2} \cos(2\pi y) - \sin\left(\frac{\pi}{2}y\right), \\ p_\Gamma^3 &= \xi\sqrt{2} \cos(2\pi x) - \cos\left(\frac{\pi}{2}x\right), & p_\Gamma^4 &= \xi\sqrt{2} \cos(2\pi y) - \cos\left(\frac{\pi}{2}y\right). \end{aligned}$$

Note that, with this choice, pressure continuity at the intersection point (8) is ensured by the fact that $\cos(\frac{\pi}{4}) = \sin(\frac{\pi}{4})$. However, flux conservation does not hold, so that we need to modify the right-hand-side of our formulation as in (35). Finally the source terms for the fracture problems are chosen accordingly as

$$\begin{aligned} f_\Gamma^1 &= \cos(2\pi x) \left[\frac{\sqrt{2}\pi}{2\ell_1} + 4\pi^2 \xi \sqrt{2} \boldsymbol{\nu}_{\gamma_1}^\tau \right] - \boldsymbol{\nu}_{\gamma_1}^\tau \frac{\pi^2}{4} \sin\left(\frac{\pi}{2}x\right), \\ f_\Gamma^2 &= \cos(2\pi y) \left[\frac{\sqrt{2}\pi}{2\ell_2} + 4\pi^2 \xi \sqrt{2} \boldsymbol{\nu}_{\gamma_2}^\tau \right] - \boldsymbol{\nu}_{\gamma_2}^\tau \frac{\pi^2}{4} \sin\left(\frac{\pi}{2}y\right), \\ f_\Gamma^3 &= \cos(2\pi x) \left[\frac{\sqrt{2}\pi}{2\ell_3} + 4\pi^2 \xi \sqrt{2} \boldsymbol{\nu}_{\gamma_3}^\tau \right] - \boldsymbol{\nu}_{\gamma_3}^\tau \frac{\pi^2}{4} \cos\left(\frac{\pi}{2}x\right), \\ f_\Gamma^4 &= \cos(2\pi y) \left[\frac{\sqrt{2}\pi}{2\ell_4} + 4\pi^2 \xi \sqrt{2} \boldsymbol{\nu}_{\gamma_4}^\tau \right] - \boldsymbol{\nu}_{\gamma_4}^\tau \frac{\pi^2}{4} \cos\left(\frac{\pi}{2}y\right). \end{aligned}$$

We perform two simulations choosing the values of the physical coefficients as:

- in case (a) we take $\nu_{\gamma_k}^\tau = \nu_{\gamma_k}^n = k \cdot 10^k$ and $\ell_k = \frac{2}{\pi} \nu_{\gamma_k}^n$, for $k = 1, 2, 3, 4$;
- in case (b) we take $\nu_{\gamma_k}^\tau = k \cdot 10^k$, $\ell_k = k \cdot 10^{-k}$ and $\nu_{\gamma_k}^n = \frac{\pi}{2} \ell_k$, for $k = 1, 2, 3, 4$.

In Figure 12(a) we show the computed numerical solution for the problem in the bulk, with the coefficients as in case (a). In Figure 12(b) we show the values of the fracture pressures as lines in the $3d$ space. Pressure continuity at the intersection point is clearly observed.

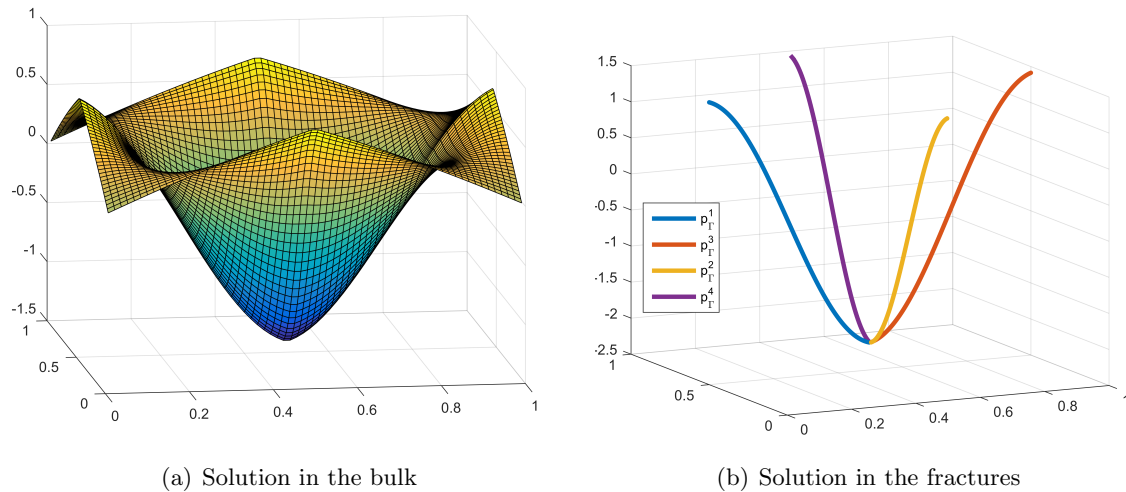


Figure 12: Example 4: Computed bulk pressure (left) and computed fracture pressures plotted as $3d$ -lines (right).

In Figures 6(a)-6(b) we report the computed errors $\|p - p_h\|_{b,DG}$ and $\|p_\Gamma - p_{\Gamma,h}\|_{\Gamma,DG}$ in loglog scale for the bulk and fracture problems, respectively, as a function of the inverse of the mesh size $1/h$. On the left we show the results obtained for test case (a) and on the right for the case (b). Again, a convergence of order 2 is observed for both $\|p - p_h\|_{b,DG}$ and $\|p_\Gamma - p_{\Gamma,h}\|_{\Gamma,DG}$, while a convergence of order 3 is observed for the error in the L^2 -norm.

References

- [1] C. Alboin, J. Jaffré, J. E. Roberts, and C. Serres. Modeling fractures as interfaces for flow and transport in porous media. In *Fluid flow and transport in porous media: mathematical and numerical treatment (South Hadley, MA, 2001)*, volume 295 of *Contemp. Math.*, pages 13–24. Amer. Math. Soc., Providence, RI, 2002.
- [2] C. Alboin, J. Jaffré, J. E. Roberts, X. Wang, and C. Serres. Domain decomposition for some transmission problems in flow in porous media. In *Numerical treatment of multiphase flows in porous media*, volume 552 of *Lecture Notes in Phys.*, pages 22–34. Springer, Berlin, 2000.

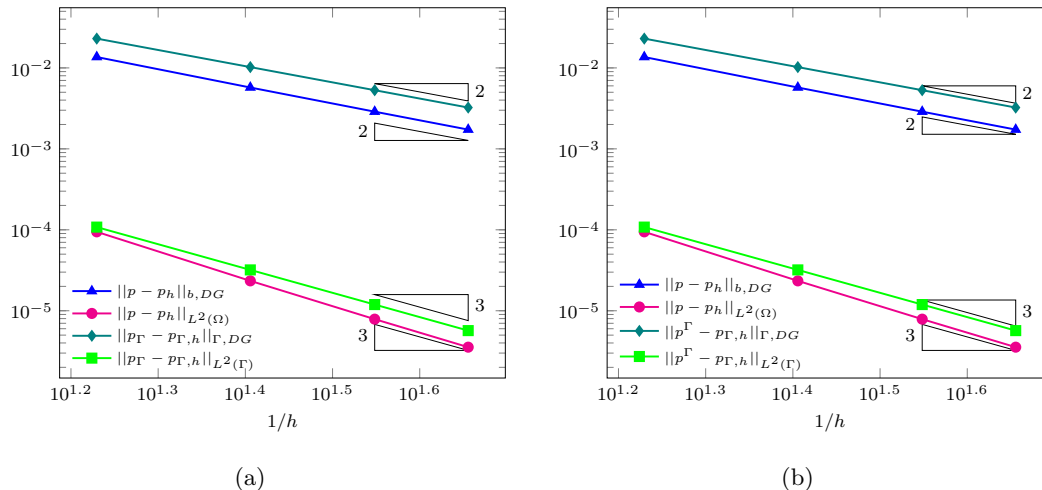


Figure 13: Example 4: Computed errors in the bulk and in the fractures as a function of the inverse of the mesh size (loglog scale). Case (a) on the left and case (b) on the right.

- [3] P. Angot, F. Boyer, and F. Hubert. Asymptotic and numerical modelling of flows in fractured porous media. *M2AN Math. Model. Numer. Anal.*, 43(2):239–275, 2009.
- [4] P. F. Antonietti, A. Cangiani, J. Collis, Z. Dong, E. H. Georgoulis, S. Giani, and P. Houston. *Review of discontinuous Galerkin Finite Element Methods for partial differential equations on complicated domains*, volume 114 of *Lecture Notes in Computational Science and Engineering*, chapter 8, pages 281 – 310. Springer, 1st edition, 2016.
- [5] P. F. Antonietti, A. Dedner, P. Madhavan, S. Stangalino, B. Stinner, and M. Verani. High order discontinuous galerkin methods for elliptic problems on surfaces. *SIAM Journal on Numerical Analysis*, 53(2):1145–1171, 2015.
- [6] P. F. Antonietti, C. Facciola, A. Russo, and M. Verani. Discontinuous Galerkin Approximation of Flows in Fractured Porous Media on Polytopic Grids. *SIAM J. Sci. Comput.*, 41(1):A109–A138, 2019.
- [7] P. F. Antonietti, C. Facciola, and M. Verani. Unified analysis of Discontinuous Galerkin approximations of flows in fractured porous media on polygonal and polyhedral grids. *Mathematics in Engineering*, to appear, 2020.
- [8] P. F. Antonietti, L. Formaggia, A. Scotti, M. Verani, and N. Verzotti. Mimetic Finite Difference approximation of flows in fractured porous media. *ESAIM Math. Model. Numer. Anal.*, 50(3):809–832, 2016.

- [9] P. F. Antonietti, S. Giani, and P. Houston. *hp*-version Composite Discontinuous Galerkin methods for elliptic problems on complicated domains. *SIAM Journal on Scientific Computing*, 35(3):A1417–A1439, 2013.
- [10] P. F. Antonietti, S. Giani, and P. Houston. Domain decomposition preconditioners for discontinuous Galerkin methods for elliptic problems on complicated domains. *Journal of Scientific Computing*, 60(1):203–227, 2014.
- [11] D. N. Arnold. An interior penalty finite element method with discontinuous elements. *SIAM J. Numer. Anal.*, 19(4):742–760, 1982.
- [12] D. N. Arnold, F. Brezzi, B. Cockburn, and L. D. Marini. Unified analysis of discontinuous Galerkin methods for elliptic problems. *SIAM J. Numer. Anal.*, 39(5):1749–1779, 2001/02.
- [13] M. F. Benedetto, S. Berrone, S. Pieraccini, and S. Scialò. The Virtual Element Method for discrete fracture network simulations. *Computer Methods in Applied Mechanics and Engineering*, 280:135–156, 2014.
- [14] M. F. Benedetto, S. Berrone, and S. Scialò. A globally conforming method for solving flow in discrete fracture networks using the Virtual Element Method. *Finite Elements in Analysis and Design*, 109:23–36, 2016.
- [15] W. M. Boon, J. M. Nordbotten, and I. Yotov. Robust discretization of flow in fractured porous media. *SIAM Journal on Numerical Analysis*, 56(4):2203–2233, 2018.
- [16] K. Brenner, J. Hennicker, R. Masson, and P. Samier. Gradient discretization of hybrid-dimensional Darcy flow in fractured porous media with discontinuous pressures at matrix–fracture interfaces. *IMA Journal of Numerical Analysis*, 37(3):1551–1585, 2016.
- [17] E. Burman, P. Hansbo, M. G. Larson, and K. Larsson. Cut finite elements for convection in fractured domains. *Computers & Fluids*, 179:726–734, 2019.
- [18] A. Cangiani, Z. Dong, and E. H. Georgoulis. *hp*-version space-time discontinuous Galerkin methods for parabolic problems on prismatic meshes. *SIAM Journal on Scientific Computing*, 39(4):A1251–A1279, 2017.
- [19] A. Cangiani, Z. Dong, E. H. Georgoulis, and P. Houston. *hp*-version discontinuous Galerkin methods for advection-diffusion-reaction problems on polytopic meshes. *ESAIM Math. Model. Numer. Anal.*, 50(3):699–725, 2016.

- [20] A. Cangiani, Z. Dong, E. H. Georgoulis, and P. Houston. *hp-version discontinuous Galerkin methods on polytopic meshes*. SpringerBriefs in Mathematics. Springer International Publishing, 2017.
- [21] A. Cangiani, E. H. Georgoulis, and P. Houston. *hp-version discontinuous Galerkin methods on polygonal and polyhedral meshes*. *Math. Models Methods Appl. Sci.*, 24(10):2009–2041, 2014.
- [22] F. A. Chave, D. Di Pietro, and L. Formaggia. A Hybrid High-Order method for Darcy flows in fractured porous media. *SIAM J. Sci. Comput.*, 40(2):A1063–A1094, 2018.
- [23] A. Y. Chernyshenko and M. A. Olshanskii. An unfitted finite element method for the darcy problem in a fracture network. *arXiv preprint arXiv:1903.06351*, 2019.
- [24] C. D’Angelo and A. Scotti. A mixed finite element method for darcy flow in fractured porous media with non-matching grids. *ESAIM: Mathematical Modelling and Numerical Analysis*, 46(02):465–489, 2012.
- [25] A. Dedner, P. Madhavan, and B. Stinner. Analysis of the discontinuous galerkin method for elliptic problems on surfaces. *IMA Journal of Numerical Analysis*, 33(3):952–973, 2013.
- [26] B. Flemisch, A. Fumagalli, and A. Scotti. A review of the XFEM-based approximation of flow in fractured porous media. In *Advances in Discretization Methods*, pages 47–76. Springer, 2016.
- [27] L. Formaggia, A. Fumagalli, A. Scotti, and P. Ruffo. A reduced model for darcy’s problem in networks of fractures. *ESAIM: Mathematical Modelling and Numerical Analysis*, 48(4):1089–1116, 2014.
- [28] L. Formaggia, A. Scotti, and F. Sottocasa. Analysis of a mimetic finite difference approximation of flows in fractured porous media. *ESAIM Math. Model. Numer. Anal.*, 52(2):595–630, 2018.
- [29] N. Frih, J. E. Roberts, and A. Saada. Modeling fractures as interfaces: a model for Forchheimer fractures. *Comput. Geosci.*, 12(1):91–104, 2008.
- [30] A. Fumagalli, E. Keilegavlen, and S. Scialò. Conforming, non-conforming and non-matching discretization couplings in discrete fracture network simulations. *Journal of Computational Physics*, 376:694–712, 2019.

- [31] A. Fumagalli and A. Scotti. A numerical method for two-phase flow in fractured porous media with non-matching grids. *Advances in Water Resources*, 62, Part C:454–464, 2013.
- [32] V. Martin, J. Jaffré, and J. E. Roberts. Modeling fractures and barriers as interfaces for flow in porous media. *SIAM J. Sci. Comput.*, 26(5):1667–1691, 2005.
- [33] N. Schwenck, B. Flemisch, R. Helmig, and B. I. Wohlmuth. Dimensionally reduced flow models in fractured porous media: crossings and boundaries. *Computational Geosciences*, 19(6):1219–1230, 2015.
- [34] E. M. Stein. *Singular integrals and differentiability properties of functions*, volume 2. Princeton university press, 1970.
- [35] G. Strang and G. J. Fix. *An analysis of the finite element method*, volume 212. Prentice-Hall Englewood Cliffs, NJ, 1973.
- [36] M. F. Wheeler. An elliptic collocation-finite element method with interior penalties. *SIAM J. Numer. Anal.*, 15(1):152–161, 1978.

MOX Technical Reports, last issues

Dipartimento di Matematica
Politecnico di Milano, Via Bonardi 9 - 20133 Milano (Italy)

- 06/2020** Domanin, M.; Piazzoli, G.; Trimarchi, S.; Vergara, C.
Image-based displacements analysis and computational blood dynamics after endovascular aneurysm repair
- 07/2020** Fumagalli, A.; Scotti, A.
Reactive flow in fractured porous media
- 04/2020** Didkovskiy, O.; Azzone, G.; Menafoglio A.; Secchi P.
Social and material vulnerability in the face of seismic hazard: an analysis of the Italian case
- 05/2020** Artioli, E.; Beiraoda Veiga, L.; Verani, M.
An adaptive curved virtual element method for the statistical homogenization of random fibre-reinforced composites
- 03/2020** Ferro, N.; Micheletti, S.; Perotto, S.
Compliance-stress constrained mass minimization for topology optimization on anisotropic meshes
- 02/2020** Fresca, S.; Dede', L.; Manzoni, A.
A comprehensive deep learning-based approach to reduced order modeling of nonlinear time-dependent parametrized PDEs
- 01/2020** Pozzi, S.; Vergara, C.
Mathematical and numerical models of atherosclerotic plaque progression in carotid arteries
- 58/2019** Antonietti, P.F.; Manzini, G.; Mourad, H.M.; Verani, M.
The virtual element method for linear elastodynamics models. Design, analysis, and implementation
- 57/2019** Antonietti, P.F.; Bertoluzza, S.; Prada, D.; Verani M.
The Virtual Element Method for a Minimal Surface Problem
- 56/2019** Antonietti, P.F.; Berrone, S.; Borio A.; D'Auria A.; Verani, M.; Weisser, S.
Anisotropic a posteriori error estimate for the Virtual Element Method